Preprints (www.preprints.org) | NOT PEER-REVIEWED | Posted: 18 September 2020

Allanites in the Sin Quyen IOCG deposit, North Vietnam

Chau Nguyen Dinh[1], Jadwiga Pieczonka[1], Adam Piestrzyński[1,*], Phon Le Khanh[2], Hao Duong Van[2]

[1] AGH University of Science and Technology; cnd@agh.edu.pl; jpeczon@agh.edu.pl; piestrz@agh.edu.pl

[2] Hanoi University of Mining and Geology; lekanhphon.humg@gmail.com; haodnth@gmail.com

[2] * Correspondence: piestrz@agh.edu.pl;Tel.: +48 12 6172433

Received: date; Accepted: date; Published: date

Abstract: Allanite minerals are the principal host of REEs in the Sin Quyen, Iron Oxide Copper Gold (IOCG) type deposit. The geochemical characteristics of these minerals are discussed in this work. The studied allanites have an unstable concentration of all major elements, such as REE (14-27 wt%), Ca (9-16 wt%), Al (8-19 wt%), Si (26-34 wt%) and Fe (12-21 wt%). Two different varieties of these minerals are documented, the older with higher REE concentrations ranging from 20 to 27 wt%, and younger with lower total REE concentration ranging from 14 to 19 wt%, which occur as a rim surrounding the older. Differences between the two groups of allanites are documented by Raman spectra and optical properties. The WDS chemical composition indicate that the allanites belong to the Ce-La-ferriallanite family, with low ΣHREE with an average of 0.21 wt.%. This work also supports the estimated timing of the deposit development focusing on detailed petrological study, and documented chemical composition of allanites confirmed by simplified statistical analysis. Temperature 355ºC which was calculated using value of $\delta^{34}S$ isotopes is interpreted as a temperature of the second crystallization stage of allanite group. The pressure of crystallization solution was calculated and is ranging from 0.98 to 5.88 MPa.

Keywords: allanite**;** REE; ore minerals; IOCG deposit; North Vietnam

1. Introduction

There are four deposits, Sin Quyen, Muong Hum, Nam Xe and Dong Pao, containing economic and subeconomic concentrations of Cu, Au, Ag and REE which are currently identified in North Vietnam [1]. The Sin Quyen deposit is the largest IOCG deposit in this area and is actively mined. The copper grade in the ore ranges from 0.55% to 1.93%, and the iron from a few percent up to several tens of percent [1-3]. The ore reserves of this deposit are reported as 550,000 t Cu, 334,000t REE, 843,000 t S, 34.7t Ag and 25.3 t Au [4-7]. Since 2006 the deposit has been exploited with an open cast system and the Fe- and Cu-concentrates are the final products of the magnetic and gravity flotation methods respectively. However, the Fe-concentrate is not a market product due to a high sulphur content. The annual production of over 30,000 tons of Cu, and approximately 300 kg Au as a co-product are reported, but REE until now (2020) have been not recovered [8-10].

The major minerals identified in the deposit are magnetite, pyrite, pyrrhotite, chalcopyrite, cubanite, and sphalerite. Allanite, ilmenite, marcasite, tennantite, arsenopyrite and galena are major accessory minerals, and native-Bi, bismuthinite, electrum, native gold, uraninite, and tellurides as minor constituents. This deposit is interesting from scientific point of view, since it consists of a complicated spatial distribution of various commodities and multi crystallisation stages proved by different results of dating of the absolute ages of the minerals. Due to the overlap of magmatic, hydrothermal and metamorphic processes resulting in several crystallization stages in the deposit, some topics such as their origin, ore crystallisation, relations between the major and minor elements and mineralisation are still being discussed ([1, 5-7, 11-19].

© 2020 by the author(s). Distributed under a Creative Commons CC BY license.

Preprints (www.preprints.org) | NOT PEER-REVIEWED | Posted: 18 September 2020

Allanite is the major REE carrier in the IOCG Sin Quyen deposit; bastnäsite and monazite are scarce. The REE-carrying minerals are dispersed and broadly spread in the deposit and occur in an assemblage with amphibole and epidote in massive ore [2]. According to McLean [6] and Li and Zhou [17] the older allanite mineralization was accompanied with Ca-K alteration, while the younger allanites are related to the initial stage of polymetallic ore precipitation of the polymetallic stage. The rocks hosting most of magnetite and allanite as well as sulphide extend beyond the sulphide mineralization zones [6]. This researcher also recognised two types of allanite; one is dark brown and more Fe rich, the other is younger, greyish in colour and surrounding the older mineral as a rim. Li and Zhou [12] and Li et al. [13] reported that REE are also contained in monazite-(Ce) and chevkinite-(Ce) in the study deposit, but with subordinate proportions. In our previous publication, the total sum of REE concentrations ranges from 12 ppm to more than 5,400 ppm [15]. However in individual samples the values can reach several percent [2]. The average content of LREE in the deposit is 7000 ppm and dominates in the deposit [6,15]. The average content of the ΣHREE is of the order of 9.19 ppm, and up to 44.4 ppm in the surrounding host rocks. In all papers mentioned before some of them are focused on Ce-allanite and distinction between groups of allanites did not get enough attention. To distinguish The aims of this paper are: (i) in detail description of the two varieties of allanite based on an analysis of their timing position, chemical composition and back scattered electron (BSE), as well as analysis by Raman spectroscope; (ii) attempt to constrain the conditions of formation of the older and younger allanites using $\delta^{34}S$ and other related minerals. Optical investigation show fine differencesbetween two groups of allanites. Further study enable to precisely determine nature of these phases, and statistic elaboration help to facilitate to geochemical quantitative processes.

2. Geological setting

North Vietnam is geologically divided into two parts by the Red River (Song Hong) fault system: the Indochina Block to the west, and the South China Craton to the east (Fig. 1). The Red River zone was formed as the consequence of the pre-Devonian collision between the South China and Indochina blocks and Triassic reactivation [18-21]. North-East Vietnam is mainly underlain by a mixed terrigenous-carbonate suite of Devonian age, including shale, black argillite, clayish limestone and marble [1]. The bedrocks in North-West Vietnam are dominated by Paleoproterozoic to Neoproterozoic-aged terrigenous sediments interbedded with minor carbonate and volcanic rocks [22]. These formations show ductile deformation and are covered by undeformed Late Triassic sediments. In North Vietnam, the Phan Si Pan and Day Nui Con Voi belts are forming south parts of Ailao Shan -Red River (ASRR) shear zone and constitute elements of the strata of the Red River shear zone (Fig. 1) [23, 24].

Preprints (www.preprints.org) | NOT PEER-REVIEWED | Posted: 18 September 2020

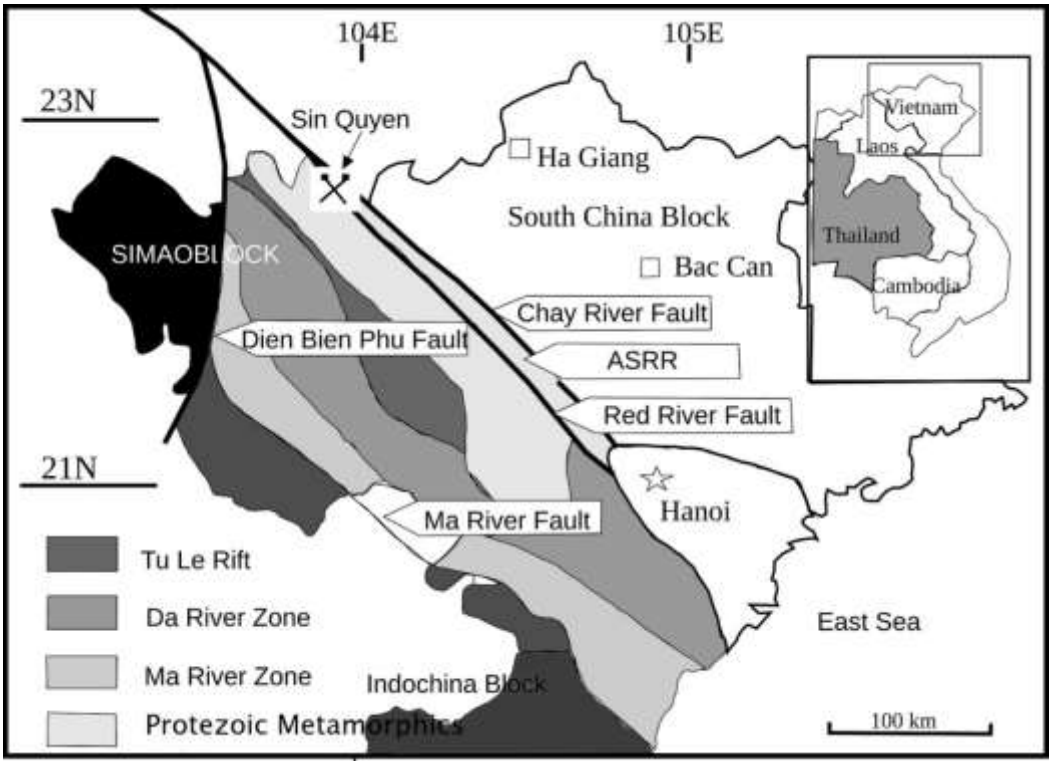

Figure 1. Geological sketch of IOCG Sin Quyen deposit follow [7], ASRR- Ailao Shan -Red River shear zone.

A part of the Phan Si Pan massive was formed by per-alkaline and meta-aluminous Po Sen-Hoa Binh plutons at 253-251 Ma of ages [21]. The Phan Si Pan Belt is a high-grade metamorphic complex including the Suoi Chieng, Sin Quyen and Cam Duong formations. The Suoi Chieng Formation is composed of Paleoproterozoic biotite schist, amphibolite and terrigenous sediments. This formation is conformably overlain by the Paleoproterozoic to Neoproterozoic-aged Sin Quyen Formation comprising terrigenous sediments interbedded with minor carbonate and volcanics. Based on the mineral composition, the Sin Quyen Formation is divided into upper and lower units (Fig. 2).

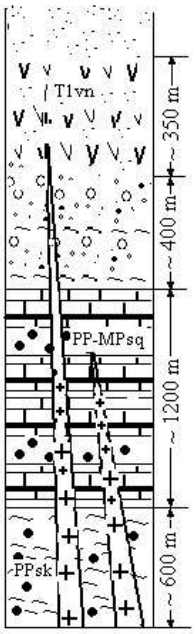

Fig. 2.Litho-Stratigraphic column of the Sin Quyen area. PPsk- Suoi Chieng metamorphosed sequence (granite, gneiss an biotite schists)– Lower Proterozoic, PP-MPsq- Sin Quyen unit (graphite schists, , mica schists, gneiss) - Tlvn – Cam Duong Formation – (marbles, limestone) Upper Proterozoic –Cambrian [2, 6].

In the upper unit, quartz (50%), graphite (15%), muscovite (12%) and biotite (10%) are the major minerals, with plagioclase, tourmaline, garnet, and sillimanite as minor components. In the lower unit, plagioclase (61%), quartz (21%), and biotite (15%) are the major minerals and apatite, sphene, calcite and garnet the accessory minerals [5,6]. The Cam Duong Formation is composed of Paleozoic suites containing quartz, sericite, graphite, carbonate and biotite (Fig. 2). The Formation strikes 280 to 320° and dips 20 to 70° the north-east [5]. The Pan Si Pan Belt complex in North-West Vietnam is intruded by Neoproterozoic and Late Permian and Early Triassic igneous rocks. The Day Nui Con Voi Belt is composed of limestone,

Preprints (www.preprints.org) | NOT PEER-REVIEWED | Posted: 18 September 2020

mafic olistoliths and mudstone matrix with slumped beds suggesting a gravity-driven chaotic sedimentation [21].

The Sin Quyen copper deposit is hosted in the Upper Sin Quyen Formation and located 300 km north-west of Hanoi, one km from the Chinese border on the right bank of the Red River. Mineralisation occurs in lenses within an elongate NW trending zone 100 – 200 m wide, nearly 2.5 km long and extending in depth to around 500 m [5]. The main mineralisation zone is strongly deformed with fractured and dislocated gneiss, mica schist and clay matrix breccia. The gneiss is principally composed of biotite, feldspar and quartz, the main composition of mica schist is biotite, muscovite, quartz and feldspar. In the mineralisation zone there are some Proterozoic granite dykes. The intrusive suites are barren of ore and basically consist of albite, biotite, and quartz [6].

The deposit is comprised of 17 lensoidal ore bodies, striking NW-SE, dipping nearly vertically (70°-90°), several to tens of metres thick (Fig. 3), and up to a few hundred metres long (Fig.4). The ore bodies often occur as ore composed of massive or banded replacement breccia. Spatial distribution of Fe, Cu and REE is highly variable. The average grade is 0.91 wt% Cu, 0.7 wt% ΣLREE (La, Ce, Pr and Nd) and 0.44 ppm Au [2,6]. From the ore geology point of view, the deposit can be divided into two zones. The first zone is principally located in the central and eastern parts, and the main minerals are chalcopyrite, pyrrhotite and pyrite, which constitute nearly 90 % of the ores with broad variations in content at different sites. The second zone dominates in the western arm; its principal minerals are magnetite, pyrite, chalcopyrite and pyrrhotite. The minerals contain from a few percent to 50 % or more of the ore. In the study deposit, allanite is the major carrier mineral for REE, bastnäsite and monazite are scarce [2, 6].

Fig. 3.Cross section through the deposit. Black rocks formed ore body marked with red lines (view towards NW, photo 2014).

3. Field and analytical methods

3.1. Samples

The samples used in this paper present encompass broad range of geological materials available in the study area: from the spoil rocks by the different sulphide skarn, massive and breccia ores up to

Preprints (www.preprints.org) | NOT PEER-REVIEWED | Posted: 18 September 2020

Cu, Fe concentrate and ore enrichment waste. The short description of every sample is provided in the Table 1. The locations of the samples were determined using a Garmin 60CSx GPS, with an accuracy of ± 2-3m and are shown on Fig. 4. From the spatial distribution of view, the samples were collected from all zones in the deposit. The samples M1-M8 were collected from the central part. Samples N1-N12 from the northern and S1-S9 from the southern part. The samples W-36, W-37 present the Cu and Fe concentrates respectively. The samples W-39, W-40 and W-41 were collected from the waste. For the study of the leaching of REE by water the samples W-48 and W-49 were collected from recent sediments along the Ngoi Phat stream.

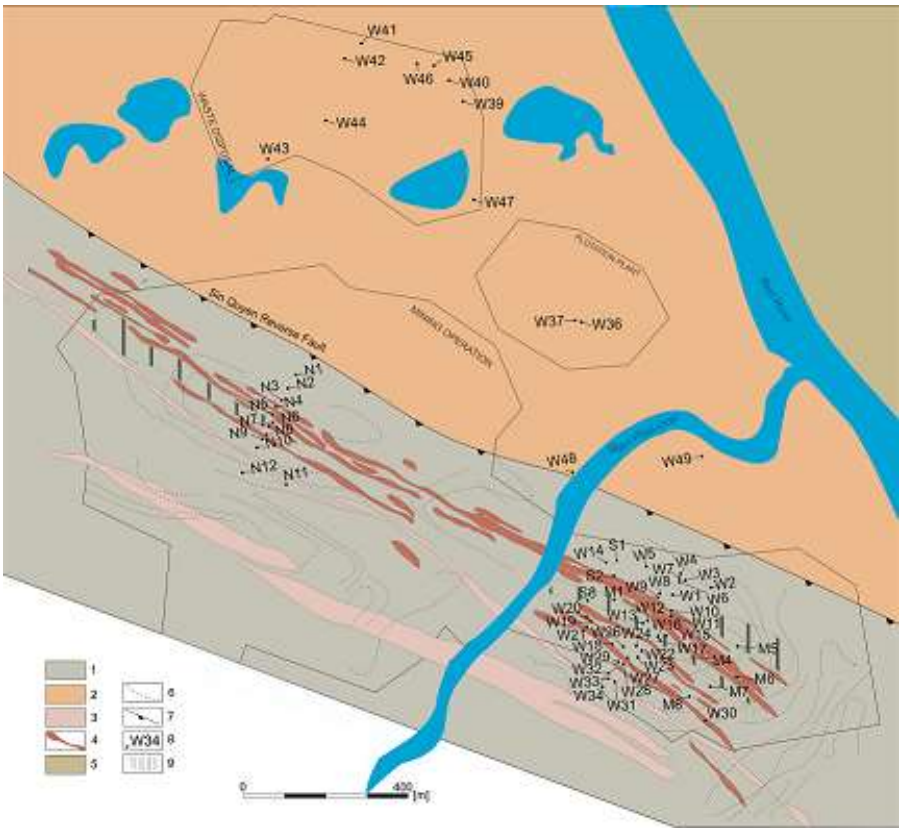

Fig.4. Position of the all samples collected during 2014 and 2015 in site visit. The background is geological map based on deposit documentation and work by Ishihara et al. [7] and Gas'kov et al. [2].

3.2. Mineralogical and chemical analysis

Analyses of ore minerals were carried out using an ore microscope and EDS system, combined with a FEI Quanta-200 FEG scanning electron microscope (20 kV acceleration voltage) and Raman spectroscopy (RS), at the laboratories of the Faculty of Geology, Geophysics and Environmental Protection AGH-University of Science and Technology in Krakow, Poland (FGGEP AGH-UST).

An ADXR AIY1100618 Raman spectroscope was used to determine the ion composition spectra of allanite. The samples were irradiated by 532 nm monochromatic photons generated by a 10 mW powered argon ion laser. The position of the Raman bands of the study samples was determined using library Raman spectra.

Bulk chemical analyses were carried out at ACME Laboratories in Vancouver Canada using the AQ251 method. A sample of 0.5 g was digested in Aqua Regia at 90°C, followed by ICP-MS. A detailed description of the analytical methodology, detection limits, and uncertainties can be

Preprints (www.preprints.org) | NOT PEER-REVIEWED | Posted: 18 September 2020

downloaded from the ACME Laboratories website at www.acmelab.com. Analytical uncertainties are typically 5% for most of the elements analysed. The detection limit for REEs varies from 0.02 ppm to 0.5 ppm, and for U and Th is equal to 0.1 ppm. The obtained chemical data were statistically processed.

3.3. REE analyses in allanites

Quantitative WDS analyses were carried out at the Critical Elements Laboratory of the FGGEP AGH-UST using a JEOL SQ8200 microprobe (EMP). For the principal elements, the following standards and measurement lines have been used: SiKα (albite), AlKα (kyanite), SKα (anhydrite), UMβ (UO_2), YLα (YPO_4), PKα(YPO_4), ScKα (100%), TiKα (rutile), CeLα ($CePO_4$), LaLα ($LaPO_4$), ThMα (ThO_2), CaKα (wollastonite), PrLβ (PrPO4), TbLα ($TbPO_4$), DyLα ($DyPO_4$), ErLα ($DyPO_4$), LuLα ($LuPO_4$), GdLβ ($GdPO_4$), PbMα (crocoite), NdLα ($NdPO_4$), SmLα ($SmPO_4$), EuLβ ($EuPO_4$), TmLα ($TmPO_4$), YbLα ($YbPO_4$), HoLβ ($HoPO_4$), AsLα (InAs). Overlap corrections of Nd-Ce, Sm-Ce, Lu-Dy, Dy-Eu, U-Th, Tm-Sm, Gd-Ho were carried out using the method described by [25] The EMP was operated in the wavelength-dispersion mode at an accelerating voltage of 15 kV, and a probe current of 40 nA, with a focused beam diameter of 3 μm. Peak/background counting times [s] were as follows: Si 10/5, Al 10/5, S 20/10, U 120/60, REE 45/15, P 20/10, Ti 20/10, Th 120/60, Ca 20/10, Pb 180/90, V 10/5, Fe 20/10 and As 20/10. The original Jeol ZAF procedures were used for a final correction of all the elements examined.

3.4. Estimation of ore crystallization temperature using sulphur isotopes

Using sulphides $\delta^{34}S$ isotopes data provided by [16] crystallization temperature was calculated. The main factors controlling a magnitude of equilibrium sulphur stable isotope fractionations are temperature, chemical composition, crystal structure and pressure [26]. For the crustal condition temperature and chemical composition are the most important, but pressure effect is minimal. The temperature factor effect quantitatively is expressed by fractionation factor $\Delta_{A\text{-}B}$ and expressed by an equation [27]:

$$\Delta_{A-B} = 1000 ln\alpha_{A-B} = \frac{\boldsymbol{a}}{T^2} + \frac{b}{T} + \boldsymbol{c} \quad (1)$$

where: $\alpha_{A\text{-}B}$ is a fractional coefficient describing relative fractionation of sulphur isotopes between substance A and B; $\boldsymbol{a}$, $\boldsymbol{b}$ and $\boldsymbol{c}$ are constants determined by theoretical analyses or experiments; T is absolute temperature [K]. The $\alpha_{A\text{-}B}$is defined as following equation:

$$\alpha_{A-B} = \frac{\left({}^{34}S/_{32}S\right)_A}{\left({}^{34}S/_{32}S\right)_B} \quad (2)$$

The constants $\boldsymbol{a}$, $\boldsymbol{b}$ and $\boldsymbol{c}$ were determined by Ohmoto and Rye [27]) for equilibrium fractionation factor for several sulphides (A) and aqueous gas H_2S (B). Following work by Ohmoto and Rye [27] for pyrrhotite (FeS) and chalcopyrite ($CuFeS_2$) $\boldsymbol{a}$=0.10 and -0.05 respectively, the constants $\boldsymbol{b}$ and $\boldsymbol{c}$ for both mentioned minerals are null. The fractionation factor between substance A and B can also be expressed by the equation:

$$\Delta_{A-B} = \delta_A - \delta_B \quad (3)$$

Preprints (www.preprints.org) | NOT PEER-REVIEWED | Posted: 18 September 2020

Parameters δ_A and δ_B are a relative fraction of the $\delta^{34}S$ with respect to Vienna-Canyon Diablo Troilite for substance A and B respectively.

For sulphides occurring in Sin Quyen IOCG deposit the measured values of $^{34}\delta$ are 8.65 ‰ and 8.27‰ for chalcopyrite and pyrrhotite respectively [16]. Therefore $\Delta_{ch\text{-}py}$ = 0.38‰. Using constant *a*, the fractionation factor between pyrrhotite (py) and chalcopyrite (ch) is:

$$\Delta_{py\text{-}ch} = \Delta_{py\text{-}H2S} - \Delta_{ch\text{-}H2S} = 1000\ln\alpha_{py\text{-}H2S} - 1000\ln\alpha_{ch\text{-}H2S} \quad (4)$$

$$\Delta_{py-ch} = \left(\frac{0.10\times10^6}{T^2}\right) - \left(\frac{-0.05\times10^6}{T^2}\right) = \frac{0{,}15\times10^6}{T^2} \quad (5)$$

Replace $\Delta_{py\text{-}ch}$ by 0.38 to the equation (5) and subtract from the obtained value of *T* (*K*) the 273 the temperature in ℃ is:

$$t(℃) = \sqrt{\frac{0.15\times10^6}{0.38}} - 273 = 355\ ℃ \quad (6)$$

3.5. Estimation of pressure

Since the depth of ore body varies from 50 to 300 m b.g.l. and the fluid density in assumption is 2 kg·dm^{-3}, the calculated hydrostatic pressure *P* [Pa] can be estimated as follow:

$$P = \rho \times h \times g \quad (7)$$

where: ρ is fluid density, *h* – depth and *g* – gravitation acceleration 9.8m·s^{-2}.

Using equation (7) the crystallization pressure of the sulphide ore could vary from 0.98 to 5.88 MPa.

4. Geochemistry of the host rock, ore, concentrates and wastes

The host rock and ore include interbedded gneisses; composed of biotite - quartz and feldspar – biotite - muscovite; quartz and feldspar mica schists; metasomatites and amphibolites, which host the mineralisation, and marbles [6]. The copper concentration ranges from several tens ppm to more than 10.0 wt% (Tab. 1) with an average of 2.56 wt% in the deposit. The iron content ranges from a single percent up to 40.0%, and reflects the combined Fe content in magnetite, silicates, pyrite and chalcopyrite (Tab. 1). Zn, Pb, Co, Ni, Mo, Sb and Se values are below 100 ppm (Tab. 1). The concentrations of Au and Ag are highly variable. Gold in the ore and rock samples ranges from a single ppb to 18.5 ppm with an average of 1.66 ppm. Silver concentrations range from 8 ppb to 4,65 ppb, with an average of 1,160 ppb (Tab. 1). High Au and Ag contents are commonly associated with massive copper ore characterised by high Cu concentration, suggesting an association of native gold with chalcopyrite and pyrite (Tab. 1). The highest concentrations of Cu, Au, Ag, Zn, Co, Se and Te are noted in the Cu concentrate, in which concentrations of Au = 6.49 ppm, Ag = 30.9 ppm (sample W-36, Tab. 1). In the magnetite concentrate an Au content of 148 ppb is noted (Tab. 1). This value is relatively high, and possibly related to the Fe bearing minerals and the sulphide contamination. The sulphur content of the magnetite concentrate reaches 3.62 wt% (Tab. 1). Such a high concentration of S showed pollution of the magnetite concentrate and explains the elevated concentration of gold that usually occurred as small inclusions in chalcopyrite and pyrite [14]. Only one sample, (W-25), shows a relatively high concentration of niobium (227 ppm). This requires further detailed study at the deposit level. No elevation of this metal is noted in either the copper or iron concentrates (samples

Preprints (www.preprints.org) | NOT PEER-REVIEWED | Posted: 18 September 2020

W-36 and W-37; Tab. 1). However a small enrichment in niobium is documented in the samples collected from the waste (samples W-39, 40 and 44; Tab. 1).

Table 1. Bulk chemical compositions of solid rocks samples Cu and Fe concentrates and wastes (ACME lab.).

Element	Fe	Mn	Co	Ni	Au	Cu	Zn	Ag	Pb	Ga	Ge	S	Marks
Units	%	ppm	ppm	ppm	ppb	ppm	ppm	ppb	ppm	ppm	ppm	%	
d.l.	0.01	1	0.10	0.10	0.20	0.01	0.10	2	0.01	0.10	0.10	0.02	
min.	0.86	114	2.30	0.10	1.60	39.00	9.10	8.00	0.89	4.00	0.10	0.02	
max.	40.0	1480	329	240	18500	>10%	196	4650	33.9	23.1	0.90	7.46	
Av.	**17.2**	**480**	**86.6**	**45.1**	**1660**	**2780**	**80.6**	**1160**	**7.23**	**12.4**	**0.51**	**1.98**	**n= 34**
St.d.	10.4	324	68.2	51.56	4030	29900	53.4	1170	8.37	5.46	0.20	1.54	
V [%]	60	68	79	114	243	107	66	100	116	44	39	78	
W-36	35.0	236	183	91.6	6490	>10%	580	30900	40.8	b.d.l.	b.d.l.	8.33	Cu-con
W-37	>40	356	135	84.8	148	998	28	230	3.56	b.d.l.	b.d.l.	3.62	Fe-con
W-39	10.6	880	46.6	26.2	68.8	555	64.3	136	4.97	b.d.l.	b.d.l.	0.66	waste I
W-40	9.57	792	36.6	24.1	67.3	386	52.2	86	4.20	b.d.l.	b.d.l.	0.6	waste II
W-44	12.2	711	30.9	20.1	167	335	42.3	86	5.31	b.d.l.	b.d.l.	0.77	Waste III

Table. 1cd

Element	Sn	Te	Tl	Bi	Cd	U	Th	Sr	V	Cs	Cr	Ti	Marks
Units	ppm	ppm	ppm	ppm	ppm	ppm	ppm	ppm	ppm	ppm	ppm	%	
d.l.	0.10	0.02	0.02	0.02	0.01	0.10	0.10	0.50	2	0.50	0.50	0.001	
min.	1.00	0.02	0.02	0.04	0.01	0.98	0.50	5.70	10.00	1.90	0.01	4.00	
max.	67.3	7.13	1.88	4.67	1.58	513	21.4	128	138	117	0.30	364	
Av.	**19.5**	**1.89**	**0.45**	**1.45**	**0.41**	**65.9**	**3.84**	**28.3**	**70.9**	**25.6**	**0.13**	**95.6**	**n= 34**
St.d.	12.4	1.72	0.44	1.26	0.41	120	4.47	30.3	30.2	22.5	0.09	92.4	
V [%]	64	91	97	87	99	182	117	107	43	88	66	97	
W-36	b.d.l.	4.91	b.d.l.	5.39	3.31	20.6	2.20	52.1	62	b.d.l.	b.d.l.	0.06	Cu-conctre
W-37	b.d.l.	0.64	b.d.l.	1.28	0.10	22.7	2.90	13.1	219	b.d.l.	b.d.l.	0.12	Fe-conctre
W-39	b.d.l.	1.04	b.d.l.	1.74	0.14	32.6	12.2	51.0	89	b.d.l.	b.d.l.	0.24	Waste I
W-40	b.d.l.	0.86	b.d.l.	1.32	0.14	30.6	8.70	45.1	83	b.d.l.	b.d.l.	0.26	Waste II
W-44	b.d.l.	0.38	b.d.l.	1.68	0.06	62.4	11.3	46.0	85	b.d.l.	b.d.l.	0.22	Waste III

Table.1. cd

Elements	Ba	Mg	Al	Na	K	Ca	Nb	Rb	Sc	Y	Marks
Units	ppm	%	%	%	%	%	ppm	ppm	ppm	ppm	
d.l.	0.50	0.01	0.01	0.01	0.01	0.01	0.02	0.01	0.02	0.01	
min.	4.00	0.03	0.30	0.01	0.02	0.30	0.08	2.50	1.00	4.24	
max.	364	5.43	8.52	4.22	4.11	29.1	2.55	294	22.0	81.4	
Av.	**95.6**	**1.24**	**2.29**	**0.28**	**1.18**	**2.40**	**1.06**	**72.7**	**4.58**	**18.6**	**n= 34**
St.d.	92.4	1.27	1.87	0.75	1.21	4.95	0.70	71.7	4.42	17.9	
V [%]	97	102	81	267	102	187	66	0.98	0.98	96	
W-36	36.1	0.32	1.07	0.24	0.29	1.90	8	b.d.l.	5	17	Cu-cont
W-37	36.5	0.42	1.35	0.42	0.37	0.53	11	b.d.l.	3	15	Fe-cont
W-39	204	1.94	6.41	1.88	2.17	3.00	33	b.d.l.	13	49	Waste I
W-40	189	1.85	6.23	1.88	2.01	2.70	37	b.d.l.	13	55	Waste II
W-44	104	1.39	5.52	1.59	1.15	2.79	35	b.d.l.	13	99	Waste III

Notes: d.l. - minimum of the detection limit. St.d. -. standard deviation; V- coefficient of variability; b.d.l. – below detection limit, Av.- Average conten

Samples W-18 and W-37 from the Fe-concentrate have relatively high vanadium values (123 and 219 ppm respectively). This can be correlated with the magnetite concentrations (Tab. 1). All of the samples are characterised by low concentrations of Ti (Tab. 1). This is typical for IOCG deposits [28-30]. REE element analyses in rock chip samples show elevated values in the samples with economic copper concentrations (Tabs. 1 and 2). However, more interesting concentrations are detected in

Preprints (www.preprints.org) | NOT PEER-REVIEWED | Posted: 18 September 2020

samples from concentrates and tailings (samples W-39, 40 and 44, Tab. 2). These values are comparable to the average REE content in the ore, because these metals are not an enrichment target, and are discarded into the waste together with the other silicates and carbonates. Only three of the 34 ore samples analysed have REE values greater than 0.2 wt% (Tab. 2). The average content of the ΣLREE is 692 ppm (for n= 34; Tab. 2), while that of ΣHREE is 9 ppm (Tab. 2). The patterns of REE distribution are presented in Figure 5. Generally, the curves can be divided into two groups. The first group is characterised by a significantly lower concentration of LREE (W-15, W-25 and W-31) when compared with the second group composed of the remaining samples.

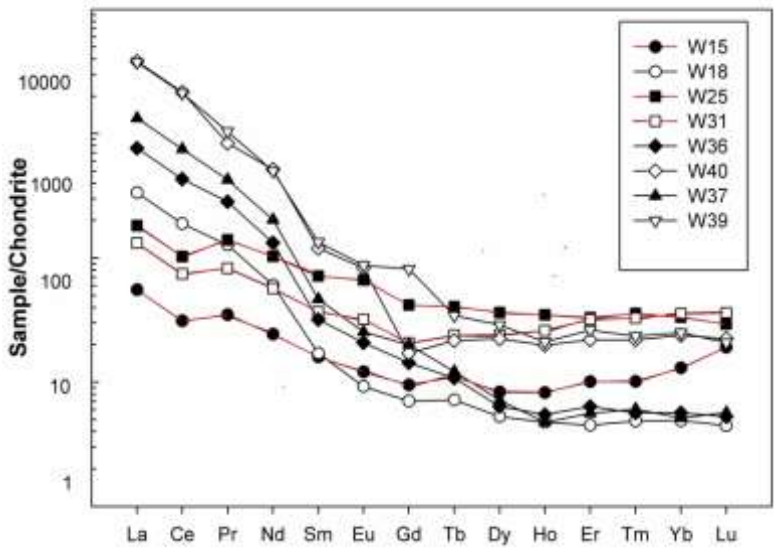

Figure 5. REE pattern based on bulk chemical analyses.

Preprints (www.preprints.org) | NOT PEER-REVIEWED | Posted: 18 September 2020

Table 2. REE bulk chemical analyses of solid rocks samples Cu and Fe concentrates and wastes (ACME lab.) in ppm.

Elements	La	Ce	Pr	Nd	Sm	Eu	Gd	Tb	Dy	Ho	Er	Tm	Yb	Lu	ΣLREE	ΣHREE	ΣREE	Marks
d.l.	0.02	0.10	0.02	0.02	0.02	0.02	0.02	0.02	0.02	0.02	0.02	0.02	0.02	0.02	0.02	0.02	0.02	
min.	5.20	7.59	1.08	3.62	0.77	0.17	0.69	0.10	0.79	0.15	0.51	0.08	0.44	0.08	19.25	2.34	21.68	
max.	831.70	1230.90	103.91	257.20	20.49	8.25	11.93	1.91	13.82	3.06	9.98	1.77	12.26	1.58	2454.62	44.38	2463.52	
Av.	**228.44**	**340.76**	**30.73**	**78.57**	**7.37**	**1.89**	**3.89**	**0.55**	**3.18**	**0.65**	**1.98**	**0.33**	**2.18**	**0.31**	**691.66**	**9.19**	**700.84**	**n= 34**
median	170.50	255.20	24.51	58.43	5.72	1.48	3.26	0.42	2.06	0.44	1.22	0.20	1.39	0.22	530.98	6.03	542.71	
St.d.	214.56	316.80	26.79	67.70	5.51	1.81	3.04	0.46	2.95	0.63	1.98	0.34	2.22	0.29	633.29	8.74	635.68	
V [%]	97	96	90	89	77	98	80	85	95	99	103	105	105	95	94	98	93	
W-36	181.30	264.69	26.41	60.56	4.72	1.17	2.85	0.39	1.57	0.30	1.02	0.14	0.91	0.13	541.70	4.46	546.16	Cu-conct
W-37	315.20	460.19	39.59	92.94	6.89	1.43	3.98	0.44	1.76	0.26	0.90	0.15	0.83	0.14	920.22	4.48	924.70	Fe-conct
W-39	887.70	1296.04	96.83	228.58	19.83	4.91	16.21	1.34	7.12	1.15	4.19	0.58	4.04	0.51	2550.10	18.93	2569.03	waste I[2]
W-40	902.60	1317.79	77.75	235.03	17.70	4.66	3.40	0.78	5.50	1.08	3.52	0.54	3.84	0.55	2558.93	15.81	2574.74	waste II[3]
W-44	1916.00	2796.78	189.15	504.94	34.56	8.70	0.31	0.99	7.31	1.46	4.71	0.71	5.21	0.65	5450.04	21.04	5471.08	wasteIII

Notes: d.l. - detection limit; St.d. standard deviation; V- coefficient of variability, Av- average content; 2. waste I–from tailing; 3. waste II from tailing; 3. Waste III - waste out from tailing.

Preprints (www.preprints.org) | NOT PEER-REVIEWED | Posted: 18 September 2020

5. Deposit mineralogy

Based on an ore microscopy investigation of polished sections of the ore samples, magnetite, pyrite, pyrrhotite, chalcopyrite, and sphalerite are the major minerals, while marcasite, tennantite, cubanite, mackinawite, arsenopyrite, galena, native-Bi, bismuthinite, electrum, native gold, molybdenite, uraninite and tellurides are the minor ones. In the publication by Li and Zhou [17] chevkinite, aeschynite, bastnäsite, epidote, titanite, zircon, F-apatite and columbite are also documented. Several styles of mineralisation are recognised in the deposit: i) massive sulphide; ii) massive magnetite; iii) mixed oxide-sulphide; iv) disseminated sulphide; and v) vein hosted. All styles are characterised by different ore mineral assemblages. Based on the local distribution of the major minerals within the deposit, Gas'kov et al. [2] divided the deposit into two zones. In the first zone, which is located in the central and eastern part of the deposit, pyrite, pyrrhotite and chalcopyrite are dominant. In the second zone, which is located in the western part of the deposit, chalcopyrite and magnetite are the principal ore minerals. In magnetite-dominant ores, chalcopyrite is very common. In the massive sulphide ore, chalcopyrite, cubanite, magnetite and pyrrhotite are the major minerals. Electrum is recognised in massive sulphide ores as 1-5 μm thick fine veinlets and as 100 μm long inclusions randomly distributed in pyrite and chalcopyrite. EDS measurements of the electrum indicate an average composition of 75.7 wt% of Au, and 24.3 wt% Ag. Some Bi-S and Bi-Te minerals were also documented using the same methods. The most important Bi-S-Te mineral is tellurobismuthite containing 87.6 wt% Bi and 21.4 wt% Te. In addition to Cu sulphides, other important accompanying minerals are allanite and uraninite, which are the major carriers of REE, and U [14-15]. Apart from REE minerals, titanite containing up to 4 % Nb (1.78 % an average from 39 WDS measurements) is also noted.

6. Results

6.1. Some remarks on the content of allanite in the deposit

Allanite is an abundant mineral in the deposit. Usually it occurs either at low concentrations, 1-2 vol%, (Figs. 6 A-E), or very rarely as a major mineral (Fig. 6F). [6] reported up to 85% of allanite in hastingsite-biotite-quartz metasomatites and up to 10% in skarns, whereas 5-7 vol% of allanite was reported in other publications [2, 7, 17] reported 5 - 30 vol% of allanite in the ore. Based on our data, both bulk chemical analyses (Tab. 2), and the mineralogical study, the average content of allanite in the ore is 0.98 wt% (Tab. 2). This was calculated following the equation: av. REE content in the ore and host rock = 0.2463% (Tab. 2) multiplied by four (25% of ΣREE in allanite itself). Based on the authors' microscopic observation of the ore, it can be concluded that allanite occurs in all styles of mineralisation. Taking into account the bulk chemical composition of the rocks and ores (Tab. 1), and 25% of ΣREE in allanite (Appendix A), it is possible to calculate the contribution in volume percent of these minerals in the investigated samples, and the calculated volume of the allanite is 4 x 0.5471% + 4 x 0.0546% + 4 x 0.0924% = 2.78%. This value of ΣREE content indicates the average concentration of allanite in the deposit. In well prepared polished sections, allanite grains can easily be identified in reflected light microscopy. Careful observation enables two different varieties of allanite to be distinguished. Both are usually present as intergrowths, with only a small difference in reflectivity and smoothness. The outer rim is characterized with lower reflectivity, close to the reflectivity of typical host minerals like feldspars and epidote, and depleted hardness. The contact between two

Preprints (www.preprints.org) | NOT PEER-REVIEWED | Posted: 18 September 2020

phases is distinct enough which suggests epitaxial overgrowing well visible also in transmitted light of the optical microscope. Allanite is typically present as subhedral grains intergrown with magnetite and amphibole (Figs. 6A, B, C, D and 6F), with titanite, biotite and sulphides (Figs. 6B, and 6E) and commonly contains inclusions of these minerals. Allanites are also present as individual isometric grains and aggregates, up to 0.6 mm in size.

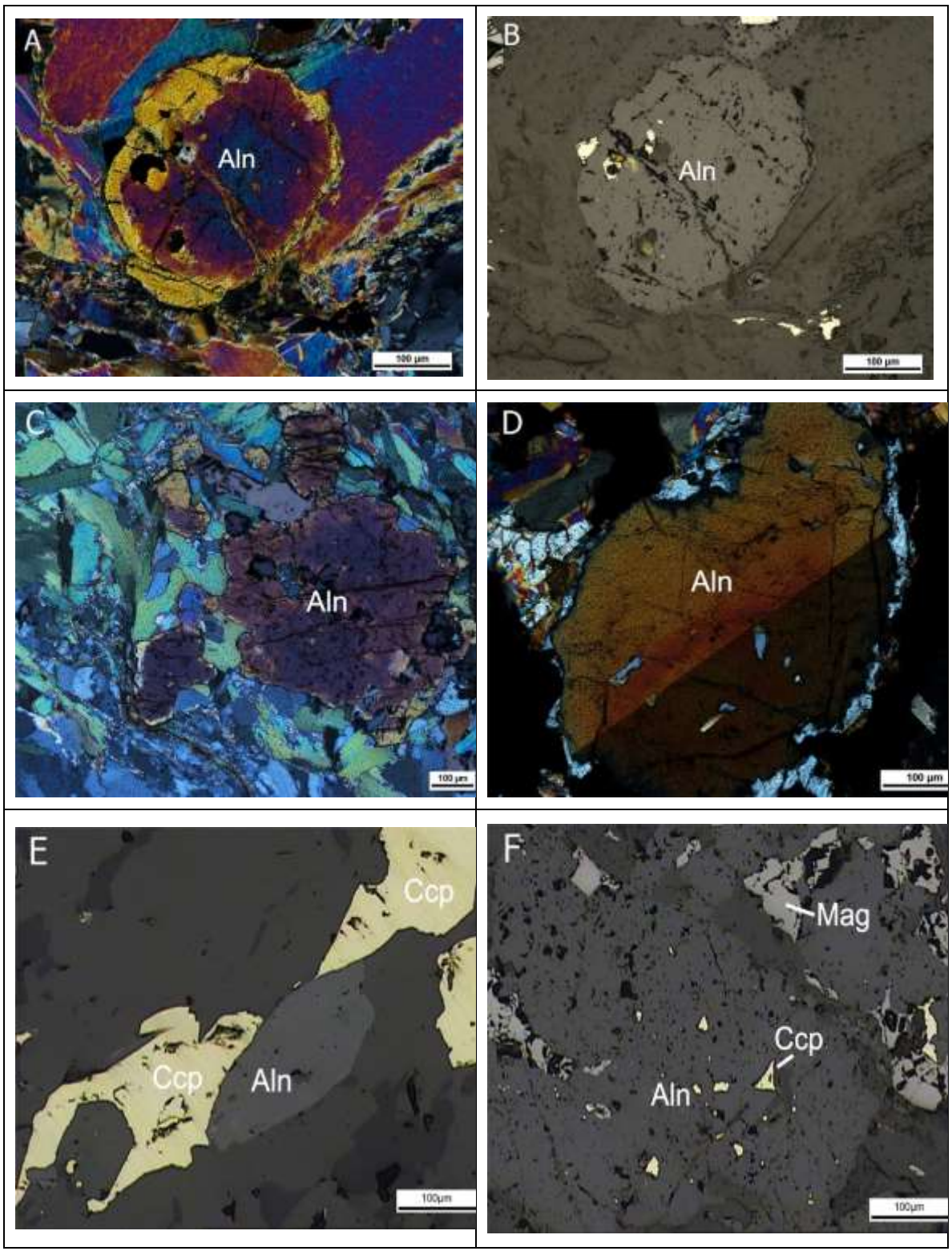

Figure 6. Microphotograph of ore minerals from Sin Quyen deposit in transmitted and reflected light.

Preprints (www.preprints.org) | NOT PEER-REVIEWED | Posted: 18 September 2020

A - allanite grain (Aln) in amphibole-biotite schist, transmitted light XN, sample N-5, B - allanite grain (Aln) in amphibole-biotite schist, white are sulphides, reflected light, sample N-5, C - allanite grains (Aln) in amphibole-biotite schist, transmitted light XN, sample N-4, D - allanite twinned crystals (Aln) in amphibole-biotite schist, transmitted light XN, sample N-4, E - intergrowth of allanite (Aln) with chalcopyrite (Cpy), in amphibole-biotite schist, reflected light, sample W-5, F- intergrowth of allanite (Aln) with magnetite (Mgt) and chalcopyrite (Cpy), reflected light, sample W-5.

6.2 Chemical composition of allanites

WDS point measurement and element maps (Figs. 7A - E and 8Al, Ca, Ce, La, Nd, Fe) show a high degree of variability in the chemical composition of the allanite grains. The basic chemical compositions of allanites are summarised in Tables 3a, 3b and Appendix A. The main characteristics of two different allanite varieties are documented in Tab. 3a and Tab. 3b. The first variety is characterised by a high ΣREE concentration of 20 – 27 wt%, with an average 24.04 wt%, and major constituents such as Si, Fe, Al and Ca (Tab. 3b). Cerium and lanthanum are the most abundant REEs. The second variety is characterised by a lower ΣREE content, ranging from 14.1 to 19.9 wt%, with an average 17.35 wt% (Tab. 3b), and by higher calcium values (Tab. 3a). The differences in allanite composition are also documented on contour WDS maps (Fig. 8). BSE images (Fig. 7A - F) also show variation in allanite compositions. The outer rim is usually depleted in Ce, La and Nd (Figs. 8C and 8D) and enriched in Ca and Al (Fig. 8Ca and 8Al). The low Fe concentration shown on Figure 8Fe makes interpretation difficult. Different grey tints are not clearly visible, and show only fine differences between two allanites (Fig. 7). The sharp borders of the outer rim suggest two stages of allanite crystallisation. This interpretation is supported by the variable chemical composition (Tabs. 3a and 3b) and textural development (Fig. 7A - F). Similar observations were also noted by McLean [6].

6.3 Raman spectroscopy of allanites

Two optically, and chemically, different allanites were examined using Raman spectroscopy. The presence of the OH group is in the broad bands at 3300 - 3100 cm^{-1} on the Raman spectra (Figs. 9 and 10) [31, 32]. In consequence the sum total of all the solid elements analysed in the allanites does not reach 100% (Tabs. 3a, 3b, and Appendix A).

A second objective of the spectroscopy is to confirm that chemical differences in the two allanites might influence both the optical properties and RS spectra (Figs. 9 and 10). The positions of RS active bands at 1100 - 300 cm^{-1} recorded for Viet-5-002 and Viet-5-001 allanite crystals differ from each other (Figs. 9 and 10), most probably due to the differences in the composition of these two phases. The main bands occur at 1052, 1045, 971 and 909 cm^{-1} (Figs. 9 and 10). The detailed RS shifts are presented in Figure 10. The bands at 1041, 1033, 957, 920, 906 and 876 cm^{-1} are attributed to SiO_2 stretching vibrations (Fig. 9). The other shifts, e.g. 685, 650, 631, 610, 601, 586, 559, 509, 445, 439,425, 413, 382, and 375, cm^{-1} of the spectral range 750 - 350 cm^{-1} are related to siloxane bending modes (Figs. 9 and 10). The Raman active bands appearing below the 350 cm^{-1} region, e.g. 310, 268, 219, 192, 126, cm^{-1} (Figs. 9 and 10), are described as lattice vibrations [33]. The location of bands attributed to SiO_2 stretching vibrations is shifted towards higher wave numbers for the Viet-5-002 crystal. The RS shifts coming from siloxane bending modes for the Viet-5-002 crystal occur at 685, 597, 563, 455, 440, 432,

Preprints (www.preprints.org) | NOT PEER-REVIEWED | Posted: 18 September 2020

419, 383 and 351 cm^{-1} and are also shifted towards higher wave numbers than for the Viet-5-001 crystal. The position of these shifts varies depending on the type of cations in the allanite-Ce-La structure (Figs. 9 and 10).

Pearson strong correlation and high variance (R^2) between CaO, Al_2O_3, ΣFeO vs ΣREE_2O_3 (Appendix B1, B2 and B3) suggest possible joined substitution of these elements by REE metals. Moderate R^2 of SiO_2 vs ΣREE_2O_3 suggests the changes in the silica composition are negligible (Appendix B4).

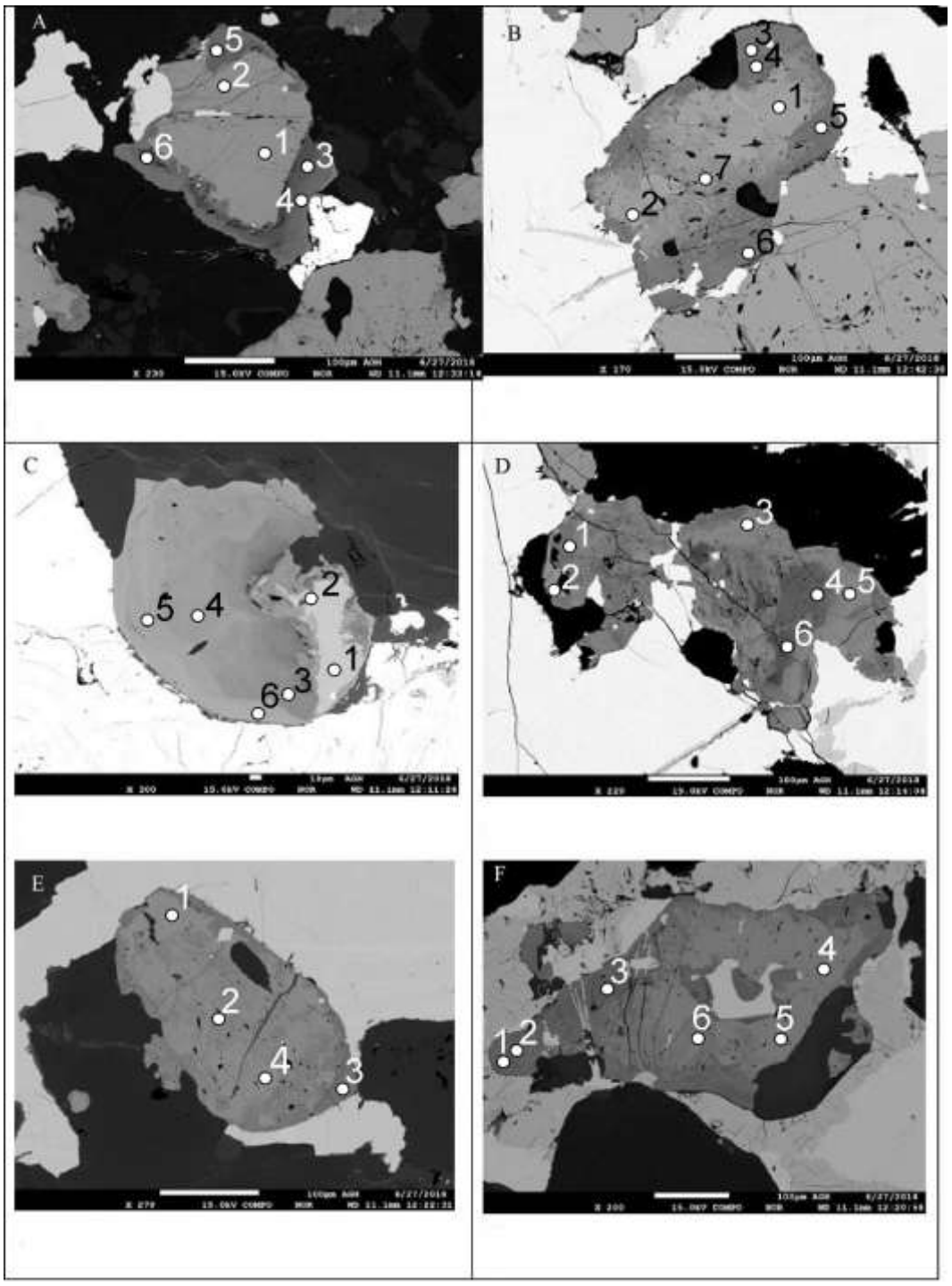

Figure 7. BSE-WDS (A-F) images of analyzed allanite grains. Gray shadows show changing in chemical composition. Numbers on pictures show positions of WDS measurements.

Preprints (www.preprints.org) | NOT PEER-REVIEWED | Posted: 18 September 2020

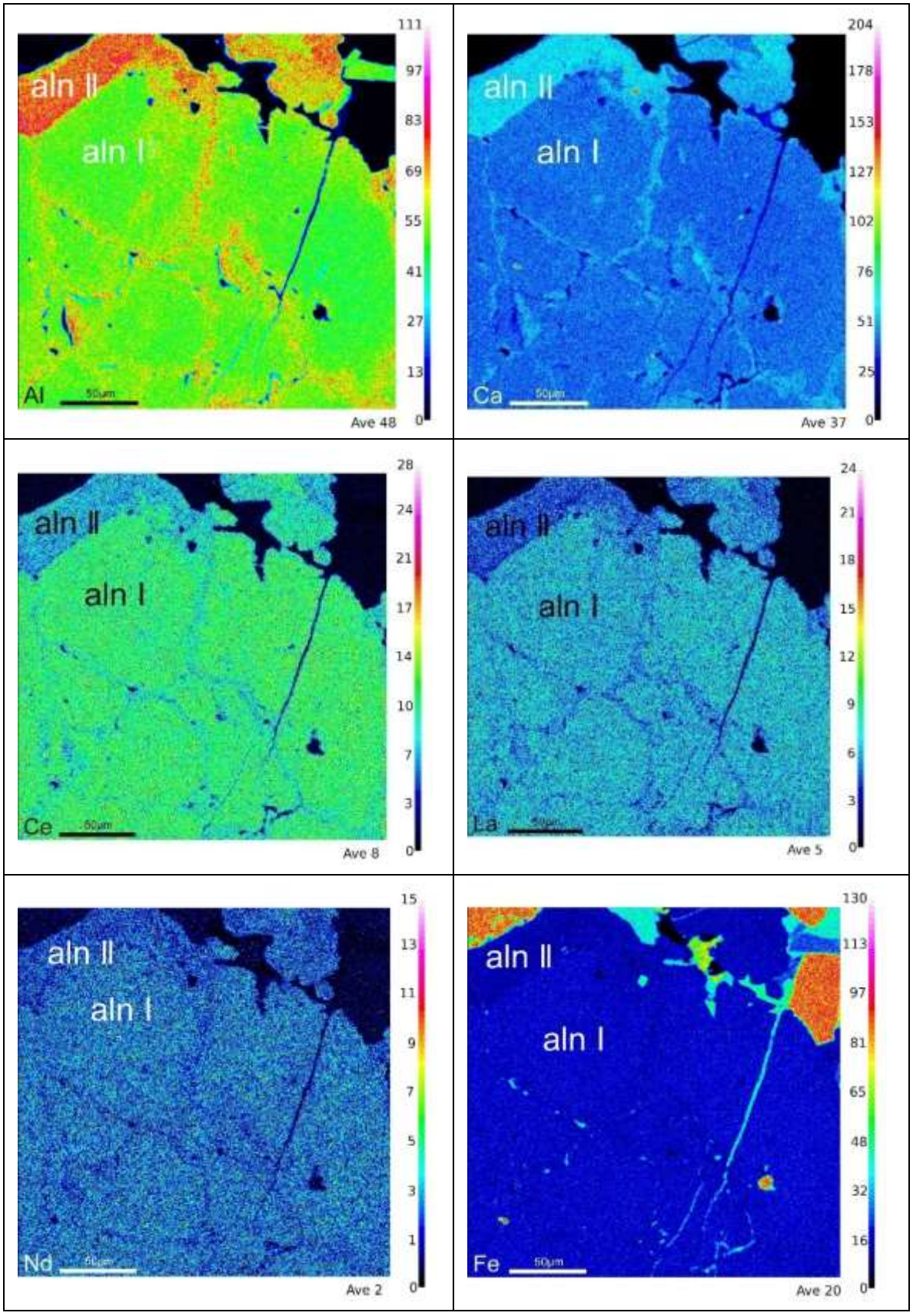

Figure 8. contour maps of two different allanites: 8Al – contour map of Al, 8Ca contour map of - Ca, 8Ce contour map of - Ce, 8La contour map of - La, 8Nd contour map of - Nd and 8F contour map of – Fe.

Preprints (www.preprints.org) | NOT PEER-REVIEWED | Posted: 18 September 2020

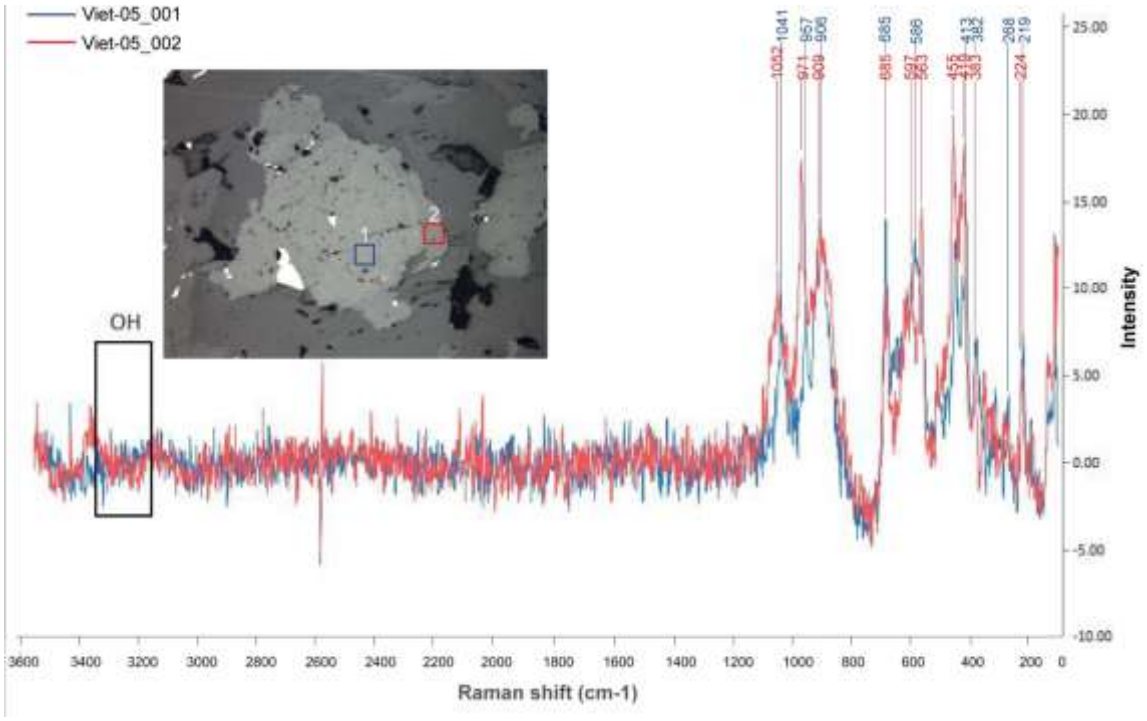

Figure 9. different allanites, 1-, 2- places of the Raman analyses, squares are 10 μm in size.

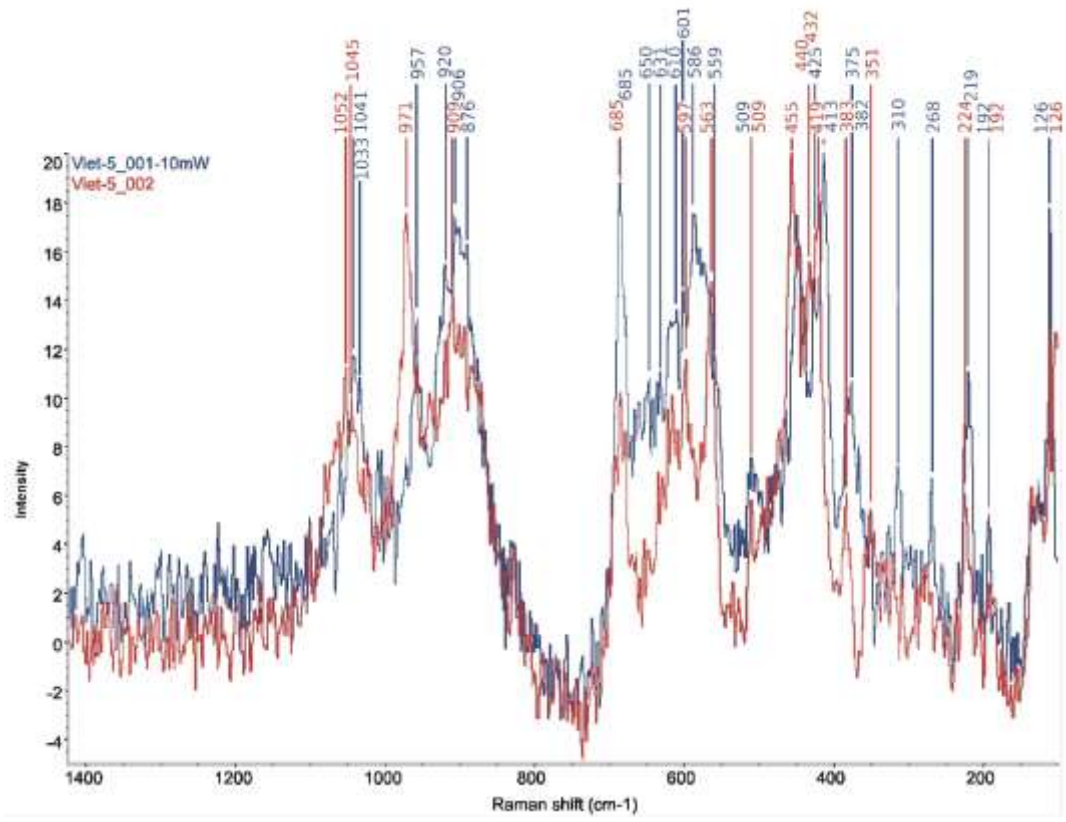

Figure 10. of two different Raman spectra of allanites, points 1and 2 form Fig.9.

Preprints (www.preprints.org) | NOT PEER-REVIEWED | Posted: 18 September 2020

7. Discussion

The highest concentrations of REE were found in the waste (samples W-39, W-40 and W-44; Table 2). However, the calculated volume of allanites in the Cu-Fe ores indicates a much lower concentration of these minerals than published in the papers [2,7, 13, 17]. In some polished sections the concentration of allanite reaches 1 to 5% by volume (e.g. sample no. W-3 - massive sulphide). The REE is present in the allanite group, monazite, chevkinite, aeschynite, bastnäsite, apatite, pyrochlore [2, 13, 17] and uraninite [16]. The average content of ΣREE in uraninites is relatively high (4.58 wt%) [15]. Allanite are most common REE minerals occurring in the deposit and surrounding rocks [2,7]. In the massive sulphide, allanite concentrations reach up to several vol%, and epidote up to 5 vol% [7]. However, the bulk chemical data (Tab. 2) show that the average content of ΣREE is low – 701 ppm. This value corresponds roughly to 2% of allanite in volume. In the study deposit the allanite group of minerals are the major carriers of REE. The other usually REE-bearing minerals are rarely observed in the ores, and their influence on the total volume of REE in the deposit is negligible. According to Gas'kov et al. [2] epidote is dominate mineral in some sections and can also contain certain amounts of REE, but it is required further investigations.

The two different allanites have also been documented through routine microscopic observation of ore. The polished surface of low REE allanite is smoother, and this mineral is also characterised by lower reflectivity and higher amounts of Al_2O_3, CaO and SiO_2 (Tab. 3a). The presence of two different allanite compositions is also visible on quantitative contour maps (Fig. 8A - F). The allanite outer rim is younger. Different tints in the grey colour show mosaic textures of allanite crystals. This can be interpreted either as a change in the fluid composition during crystallisation, or changes in the composition during Na-alteration [17]. The rim surrounding some allanite grains can be interpreted as an epitaxial allanite overgrowth from solutions with decreasing REE content during the final crystallisation phase. The chemical variability could be related to coupled substitution of REE^{3+} and Fe^{2+} by Ca^{2+} and Fe^{3+} ($REE^{3+} + Fe^{2+} \leftrightarrow Ca^{2+} + Fe^{3+}$) [7]. Variable composition of REE, and other major elements, might indicate that the allanites belong to the Ce-La-ferriallanite family. However the l4.44 wt% and 17.72 wt% average of total iron oxide (FeO) content (Tabs. 3a and 3b respectively) is related to the ferriallanite. But the alumina content (17.0 wt% and 12.4 wt%) is higher relative to this mineral stoichiometry. Statistical parameters calculated separately for the two groups of allanites show low values of standard deviation (St.d.) and coefficient of variability (V) for all the major elements (Tabs. 3a and 3b). Higher variability of both the V and St.d. parameters are recorded for most of the minor constituents (Tab. 3a and 3b). The correlations calculated for the basic elements in the allanites show good Pearson correlation between CaO, Al_2O_3, FeO and low correlation of SiO_2 vs ΣREE_2O_3 (Appendix B1, B2, B3, B4). The negative correlation of CaO and Al_2O_3 vs ΣREE might suggest replacement of both cations by the REE during hydrothermal alteration, and recrystallization. Based on the replacement model proposed in publications by Li and Zhou [17], and Li et al. [13] the mass balance calculations are difficult in the case of hydrothermal processes. Ce-Chevkinite, described in detail in the above mentioned publications, contains high ΣREE and TiO_2, and low ΣFe and SiO_2, and a total absence of alumina. In the vicinity of allanite grains no Ti-oxides are observed, and replacement textures are commonly lacking. Based on these observations, it can be suggested, that crystallisation of the allanites and chevkinite took place during different stages of the deposit development. The first group of allanite (older) was formed during the early stages of alteration

Preprints (www.preprints.org) | NOT PEER-REVIEWED | Posted: 18 September 2020

(841-836 Ma) while the second one(younger) was established during the later hydrothermal processes [16, 34]. Temperature 355ºC let to explain position of second allanite stage [17]. This stage is documented also by the presence of sulphide inclusions within the altered allanite grains (Fig. 6F). The crystallization hydrostatical pressure of the hydrothermal solutions which was responsible for sulphide ore precipitation could vary from 0.98 to 5.88 MPa . The major volume of allanite is correlated with the precipitation of magnetite [16, 17]. Association of both allanite and magnetite minerals has been confirm also in the mentioned above publications. Therefore, the oldest uraninite is dated for 575-430 Ma [16]. This ~~a~~age is also confirm by presence of REE within the magnetite [16]. Moreover, the second crystallization stage of uraninite is much younger and was dated 82-42 Ma [16]. Uraninites of this stage also contain substitutions of REE, and their chondrite normalized patterns of REE have significantly strong positive Eu and Lu anomaly in comparison with that in the older ones [16], but both older and younger confirmed presence of different stages and possible late crystallization of REE containing mineral phases [16, 35, 36].The pattern of REE in the two groups of alanites (Fig. 11) are similar to those of REE in the bulk chemical analyses of the host rocks (Fig. 5).However, the REE pattern in the Fig. 5 are smooth. It is connected with REEbroad dispersion in the host rocks, which took place during hydrothermal alteration.. Hydrothermal alteration of the host rocks was happened during the cooling of fluids responsible for ions transportation and minerals crystallization. Temperature of 355ºC might be an initial temperature of the final crystallization of minerals which were recognized as a polymetallic stage.

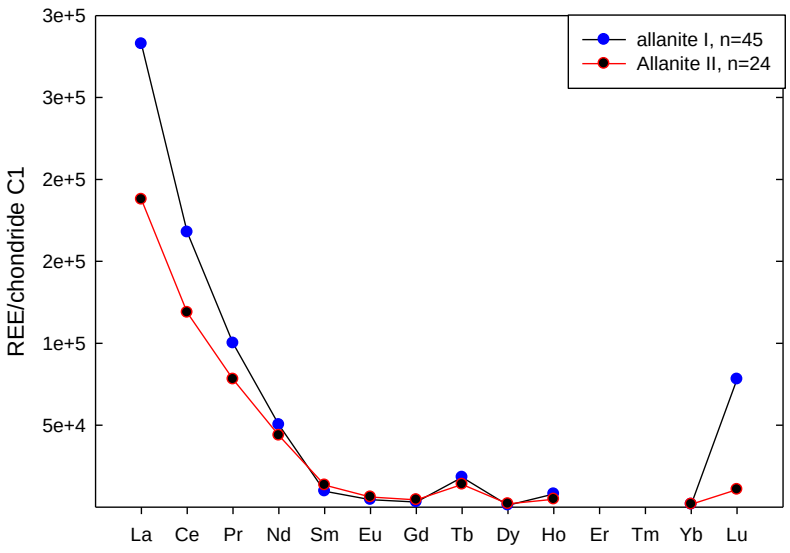

Figure 11. The REE pattern of two allanite groups.

8. Conclusions

Up to now, all the studies related to the Sin Quyen deposit have described petrological details concerning alteration processes based on the following replacement reactions chevkinite → allanite–––aeschenite and bastnäsite, monazite → fluorapatite and allanite [2, 6, 17]. Chevkinite is occurring in a significantly small quantity [17] in comparison with the common allanite, and in addition, the other reaction mentioned above played a less important role.

Preprints (www.preprints.org) | NOT PEER-REVIEWED | Posted: 18 September 2020

Allanites are the major carriers of the REE metals. The differences in chemical composition and Raman spectra characteristics clearly document the presence of two groups of allanites. The first group is characterised by a higher total REE_2O_3 content at a level of 20 wt% to 27 wt% and lower CaO and Al_2O_3 (Tab. 4). The chemical composition of the second ferriallanite group has a low total REE_2O_3 content, which ranges from 14 to 20 wt% (Tab. 4). In addition, negative correlations have been noted between two pairs of major compositions of the allanite: CaO and REE_2O_3, R= –0.85 (Appendix B1) and Al_2O_3 – REE_2O_3, R= -0.79 (Appendix B2). A positive correlation was only noted for the FeO – REE_2O_3, R= 0.76 (Appendix B3). A relatively weak correlation (R= 0.60) is observed for the pair SiO_2-REE_2O_3 (Appendix B4). Apart from silica, all the major elements show a bi-modal distribution clearly visible on histograms (Appendix C1, C2, C3, C4). Silica, having a uni-modal characteristic (Appendix C5) and very low coefficient of variability (4.1 and 3.7, rf. Tab. 3a and 3b), represents a more stable element in the allanite structure. All these correlations confirm the presence of two groups of allanite phases characterised by variable chemical composition and differences in Raman spectra. Variability in the chemical composition of the allanites can also suggest substitutions expressed as: $REE^{3+} + Fe^{2+} = Ca^{2+} + Fe^{3+}$ and $REE^{3+} + Fe^{2+} = Ca^{2+} + Al^{3+}$ [36]. A similar model was postulated following experiments carried out by [38]. The conclusion can therefore be drawn that the allanite minerals could be precipitated during different stages of the formation of the deposit.

Funding: This research received no external funding

Acknowledgement: The work was financially supported by the UST-AGH Krakow, Grants no 11.11.140.161 and 11.11.140.645 and University of Mining and Geology (UMG), Hanoi, Vietnam, Grant no. 01/2012/HD-HTQTSP. The authors are grateful to G. Kozub MSc and A. Włodek MSc from the Critical Elements Laboratory FGGEP UST-AGH Krakow for the WDS analyses and to T. Ćwiertnia MSc for preparation of the graphics.

Conflict of Interest: The authors declare no conflicts of interest. The funders had no role in the design of the study, in the collection and interpretation of data, in the writing of the manuscript, and in the declaration to publish the results.

Preprints (www.preprints.org) | NOT PEER-REVIEWED | Posted: 18 September 2020

Appendix A

WDS concentrations of rare earth element in allanite in wt%.

Nr	La_2O_3	Ce_2O_3	Pr_2O_3	Nd_2O_3	Sm_2O_3	Eu_2O_3	ΣLREE	Gd_2O_3	Tb_2O_3	Dy_2O_3	Ho_2O_3	Yb_2O_3	Lu_2O_3	ΣHREE	ΣREE	ΣLREE/ ΣHREE
1	4.43	6.95	0.56	1.66	0.16	0.04	13.8	0.11	0.04	0.08	b.d.l.	b.d.l.	0.06	0.280	14.08	49
2	3.81	7.05	0.77	2.62	0.32	0.02	14.6	0.13	0.04	0.09	0.03	b.d.l.	0.01	0.296	14.89	49
3	4.98	6.95	0.67	1.56	0.11	0.01	14.3	0.04	0.08	0.06	0.01	b.d.l.	b.d.l.	0.197	14.48	72
4	4.74	7.81	0.74	1.80	0.24	0.03	15.4	0.02	0.07	0.01	0.06	0.01	b.d.l.	0.162	15.53	95
5	5.04	7.61	0.75	1.57	0.12	b.d.l.	15.10	0.11	0.04	0.08	b.d.l.	b.d.l.	0.06	0.280	15.38	54
6	5.15	7.49	0.68	1.65	0.13	0.02	15.12	0.08	0.03	0.02	b.d.l.	0.04	0.01	0.172	15.30	88
7	4.58	7.26	0.70	1.90	0.23	0.05	14.72	0.04	0.04	b.d.l.	0.04	b.d.l.	0.01	0.126	14.85	117
8	4.30	7.95	0.87	2.93	0.32	0.07	16.43	0.12	0.07	0.07	0.02	b.d.l.	0.04	0.306	16.74	54
9	9.15	13.0	0.98	2.29	0.01	0.02	25.42	b.d.l.	0.01	0.01	0.13	0.01	b.d.l.	0.145	25.57	175
10	8.07	11.8	1.00	2.30	0.17	0.01	23.33	b.d.l.	0.02	0.02	0.05	b.d.l.	0.01	0.099	23.43	236
11	5.45	8.58	0.89	2.04	0.22	0.01	17.19	0.13	0.07	b.d.l.	b.d.l.	0.03	0.08	0.316	17.51	54
12	7.61	10.6	0.81	1.96	0.14	0.03	21.18	b.d.l.	0.05	0.05	0.02	0.01	0.01	0.135	21.32	157
13	8.53	12.9	1.04	2.29	0.11	0.05	24.88	0.05	0.04	0.04	0.01	0.02	0.01	0.159	25.04	156
14	8.81	12.5	1.06	2.46	0.14	0.03	24.99	0.03	0.12	b.d.l.	0.04	0.03	b.d.l.	0.229	25.22	109
15	8.64	12.3	0.96	2.05	0.07	0.02	24.05	0.05	0.06	0.03	b.d.l.	b.d.l.	b.d.l.	0.131	24.18	184
16	8.58	12.1	1.11	2.43	0.13	b.d.l.	24.33	0.07	0.09	0.02	b.d.l.	b.d.l.	0.02	0.194	24.53	125
17	6.02	10.2	1.10	3.06	0.27	0.02	20.69	b.d.l.	0.07	b.d.l.	0.10	b.d.l.	b.d.l.	0.169	20.86	122
18	6.12	10.8	1.16	3.34	0.24	0.05	21.75	0.16	0.05	0.04	b.d.l.	b.d.l.	b.d.l.	0.245	22.00	89
19	8.11	12.2	0.98	2.33	0.13	0.03	23.77	0.12	0.02	0.03	b.d.l.	0.02	0.01	0.203	23.97	117
20	7.91	11.6	1.15	2.44	0.19	b.d.l.	23.33	0.09	0.09	0.02	b.d.l.	0.03	0.04	0.267	23.60	87
21	8.56	12.9	1.13	2.49	0.14	0.01	25.25	b.d.l.	0.07	0.02	0.05	b.d.l.	b.d.l.	0.139	25.39	182
22	8.39	11.8	0.96	2.18	0.13	0.01	23.51	b.d.l.	0.10	0.04	0.03	0.04	b.d.l.	0.211	23.72	111
23	6.77	10.2	0.99	2.07	0.10	b.d.l.	20.16	0.09	0.04	b.d.l.	b.d.l.	0.02	0.02	0.178	20.34	113
24	8.96	12.4	1.10	2.30	0.13	0.01	24.90	0.05	0.07	b.d.l.	b.d.l.	0.02	b.d.l.	0.133	25.04	187
25	6.80	13.4	1.36	3.73	0.25	0.03	25.53	b.d.l.	0.13	b.d.l.	0.06	0.02	0.05	0.257	25.79	99
26	8.18	10.3	1.13	3.60	0.56	0.10	23.86	0.10	0.05	0.03	b.d.l.	b.d.l.	b.d.l.	0.186	24.04	128
27	3.98	8.41	1.09	3.46	0.41	0.03	17.38	0.28	0.08	b.d.l.	0.04	0.02	b.d.l.	0.420	17.80	41
28	5.06	9.11	1.03	3.17	0.34	0.02	18.73	0.24	0.05	0.09	b.d.l.	0.04	0.05	0.475	19.21	39
29	4.46	9.45	0.98	3.24	0.34	0.05	18.52	0.15	0.07	0.10	b.d.l.	0.02	b.d.l.	0.338	18.86	55
30	6.05	12.8	1.28	3.96	0.27	0.05	24.38	0.09	0.04	0.05	b.d.l.	0.02	0.01	0.207	24.58	118
31	7.97	13.4	1.29	3.27	0.16	0.03	26.11	b.d.l.	0.04	0.01	0.07	0.13	0.02	0.256	26.36	102
32	7.49	13.8	1.39	3.56	0.15	0.06	26.50	b.d.l.	0.13	0.01	b.d.l.	0.04	0.02	0.192	26.69	138
33	5.25	11.8	1.30	4.41	0.35	0.06	23.14	b.d.l.	0.07	0.04	0.04	0.09	b.d.l.	0.232	23.37	100
34	6.90	13.6	1.39	3.80	0.17	0.02	25.88	b.d.l.	0.08	0.05	0.12	0.02	b.d.l.	0.253	26.14	102
35	4.43	10.6	1.34	4.56	0.50	0.06	21.44	b.d.l.	0.05	0.02	0.06	0.09	0.04	0.266	21.71	81
36	5.27	9.05	0.95	2.63	0.34	0.05	18.29	0.20	0.11	0.11	0.02	0.11	0.03	0.575	18.86	32
37	6.13	9.57	b.d.l.	2.43	0.20	0.16	18.49	0.13	0.04	0.04	0.02	b.d.l.	b.d.l.	0.233	18.72	79

Preprints (www.preprints.org) | NOT PEER-REVIEWED | Posted: 18 September 2020

38	4.86	8.62	0.85	2.75	0.27	0.01	17.37	0.13	0.05	0.08	b.d.l.	0.01	b.d.l.	0.268	17.64	65
39	6.78	10.8	1.08	3.17	0.25	0.04	22.14	b.d.l.	0.04	0.07	0.09	b.d.l.	b.d.l.	0.202	22.34	110
40	5.46	9.73	1.11	3.04	0.27	0.07	19.67	0.08	0.04	0.04	0.04	b.d.l.	0.02	0.214	19.89	92
41	5.61	9.00	0.89	2.54	0.26	0.06	18.36	0.07	0.05	0.03	0.01	b.d.l.	0.01	0.167	18.52	110
42	9.15	12.7	1.02	2.34	0.17	b.d.l.	25.37	0.06	0.05	0.03	b.d.l.	0.02	b.d.l.	0.156	25.53	163
43	8.96	12.7	1.04	2.22	0.17	0.02	25.08	0.09	0.08	b.d.l.	b.d.l.	b.d.l.	b.d.l.	0.164	25.24	153
44	7.71	11.3	0.96	2.44	0.14	0.01	22.53	0.13	0.03	b.d.l.	b.d.l.	0.02	0.01	0.197	22.72	114
45	4.84	8.56	0.97	2.93	0.29	0.07	17.66	0.02	0.05	b.d.l.	b.d.l.	0.01	0.03	0.110	17.77	161
46	8.79	12.8	1.09	2.30	0.11	0.01	25.07	0.11	0.02	0.02	0.01	0.03	b.d.l.	0.184	25.25	136
47	7.65	11.9	1.06	2.38	0.15	b.d.l.	23.19	b.d.l.	0.10	b.d.l.	b.d.l.	0.01	b.d.l.	0.107	23.30	217
48	5.89	9.89	1.04	2.84	0.21	b.d.l.	19.86	0.03	0.09	0.03	0.02	0.01	0.01	0.173	20.04	115
49	9.08	12.6	1.02	2.47	0.14	b.d.l.	25.27	0.01	0.04	0.01	0.07	0.01	b.d.l.	0.131	25.40	193
50	8.76	12.8	1.05	2.39	0.10	0.01	25.06	0.06	0.06	b.d.l.	0.01	b.d.l.	0.05	0.182	25.24	138
51	8.62	12.2	1.04	2.55	0.08	0.04	24.52	0.03	0.07	b.d.l.	b.d.l.	b.d.l.	0.02	0.118	24.64	208
52	6.94	10.8	0.90	2.06	0.08	0.02	20.78	0.03	0.08	b.d.l.	b.d.l.	b.d.l.	b.d.l.	0.108	20.89	192
53	6.73	9.55	0.84	1.96	0.12	0.01	19.22	0.01	0.04	0.06	b.d.l.	0.05	b.d.l.	0.145	19.37	133
54	8.97	13.5	1.08	2.54	0.13	0.02	26.20	0.03	0.07	0.04	b.d.l.	b.d.l.	0.01	0.148	26.34	177
55	9.02	12.4	0.94	2.55	0.11	0.04	25.05	0.08	0.05	b.d.l.	b.d.l.	0.02	0.01	0.159	25.20	158
56	8.65	12.7	1.07	2.23	0.05	0.02	24.73	0.01	0.09	b.d.l.	0.05	0.03	0.01	0.177	24.91	140
57	7.85	12.7	1.16	2.46	0.11	0.01	24.31	b.d.l.	0.06	b.d.l.	0.02	0.01	b.d.l.	0.099	24.41	246
58	5.34	8.41	0.75	2.00	0.22	0.05	16.76	0.08	0.06	0.01	0.01	b.d.l.	0.01	0.164	16.93	102
59	8.36	12.4	1.15	2.52	0.16	0.01	24.57	0.12	0.04	0.06	0.05	0.01	b.d.l.	0.280	24.85	88
60	5.76	8.54	0.68	1.96	0.12	0.05	17.11	0.02	0.07	b.d.l.	b.d.l.	0.03	0.01	0.129	17.24	133
61	6.58	9.30	0.95	2.16	0.21	0.02	19.21	0.11	0.04	0.03	b.d.l.	0.01	b.d.l.	0.182	19.39	106
62	8.88	12.8	1.21	2.44	0.13	0.01	25.48	0.08	0.09	0.07	0.01	b.d.l.	b.d.l.	0.243	25.72	105
63	8.78	13.0	1.11	2.31	0.10	b.d.l.	25.28	0.01	0.11	0.02	b.d.l.	b.d.l.	0.02	0.163	25.44	155
64	9.16	13.0	1.08	2.53	0.09	0.01	25.83	0.06	0.05	0.02	b.d.l.	0.03	b.d.l.	0.157	25.99	165
65	6.94	10.2	0.89	2.36	0.20	0.04	20.66	b.d.l.	0.09	0.06	0.04	b.d.l.	b.d.l.	0.190	20.85	109
66	6.52	9.96	0.95	1.99	0.18	0.01	19.60	b.d.l.	0.08	0.02	0.06	b.d.l.	b.d.l.	0.155	19.75	126
67	6.19	9.67	0.83	1.97	0.12	0.01	18.80	0.04	0.07	b.d.l.	b.d.l.	b.d.l.	0.02	0.136	18.93	138
68	6.86	10.0	0.86	2.15	0.18	0.06	20.16	0.17	0.07	0.05	b.d.l.	b.d.l.	0.04	0.330	20.49	61
69	8.46	12.1	1.03	2.38	0.13	b.d.l.	24.09	0.07	0.11	0.01	b.d.l.	b.d.l.	0.04	0.223	24.31	108
min.	3.81	6.95	b.d.l.	1.56	0.01	b.d.l.	13.80	b.d.l.	0.01	b.d.l.	b.d.l.	b.d.l.	b.d.l.	0.099	14.08	32
max.	9.16	13.8	1.39	4.56	0.56	0.16	26.50	0.28	0.13	0.11	0.13	0.13	0.08	0.575	26.69	246
Av.	**6.94**	**10.8**	**0.99**	**2.56**	**0.19**	**0.03**	**21.53**	**0.06**	**0.06**	**0.03**	**0.02**	**0.02**	**0.013**	**0.206**	**21.73**	**120.478**
St. d.	1.63	1.96	0.21	0.63	0.10	0.03	3.67	0.06	0.03	0.03	0.03	0.03	0.018	0.085	3.648	47.887
V [%]	23.5	18.2	21.5	24.7	52.9	97.7	17.1	97.0	41.7	101	144	156	145	41.3	16.8	39.7

Notes: Sought but no detected: Er. Tm; Av.- average content; V- coefficient of variability; St. d. – standard deviation; b.d.l. – below detection limit.

Preprints (www.preprints.org) | NOT PEER-REVIEWED | Posted: 18 September 2020

Appendix B1. Correlation between CaO and **ΣREE$_2$O$_3$**

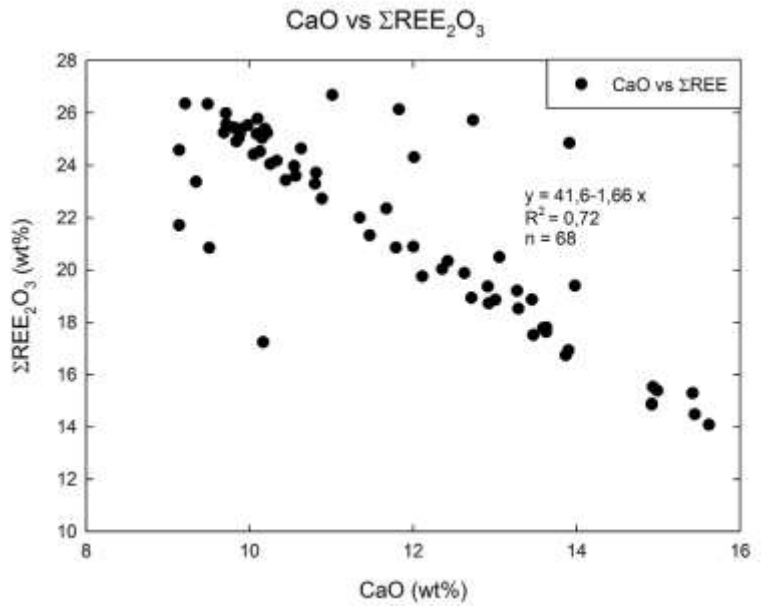

Appendix B2. Correlation between Al$_2$O$_3$ and **ΣREE$_2$O$_3$**

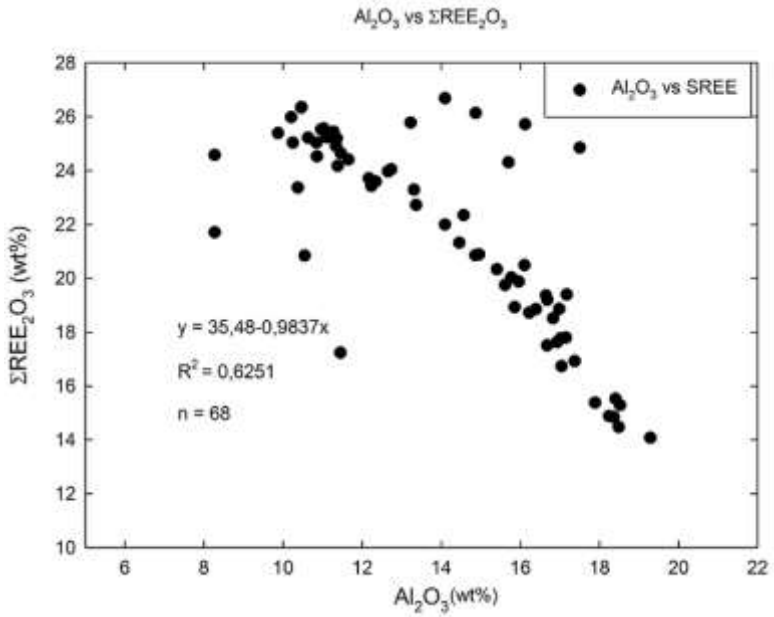

Preprints (www.preprints.org) | NOT PEER-REVIEWED | Posted: 18 September 2020

Appendix B3. Correlation between FeO and **ΣREE$_2$O$_3$**

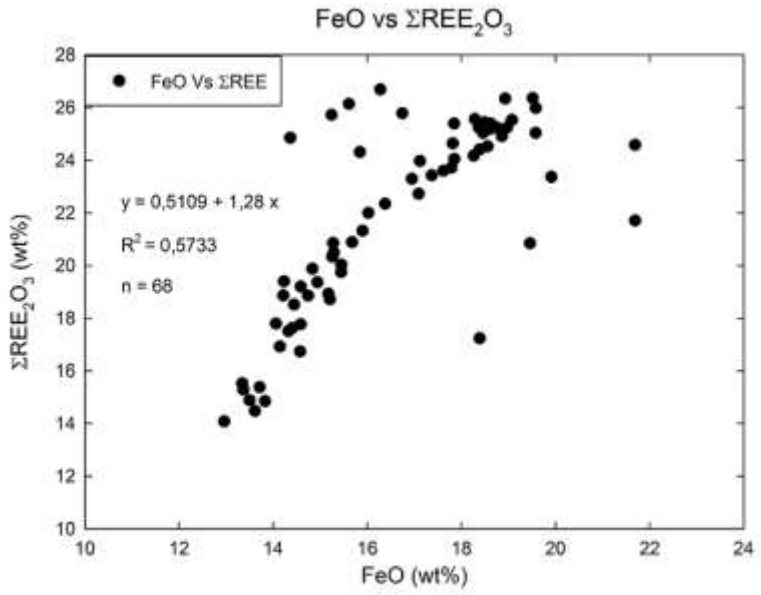

Appendix B4. Correlation between SiO$_2$ and **ΣREE$_2$O$_3$**

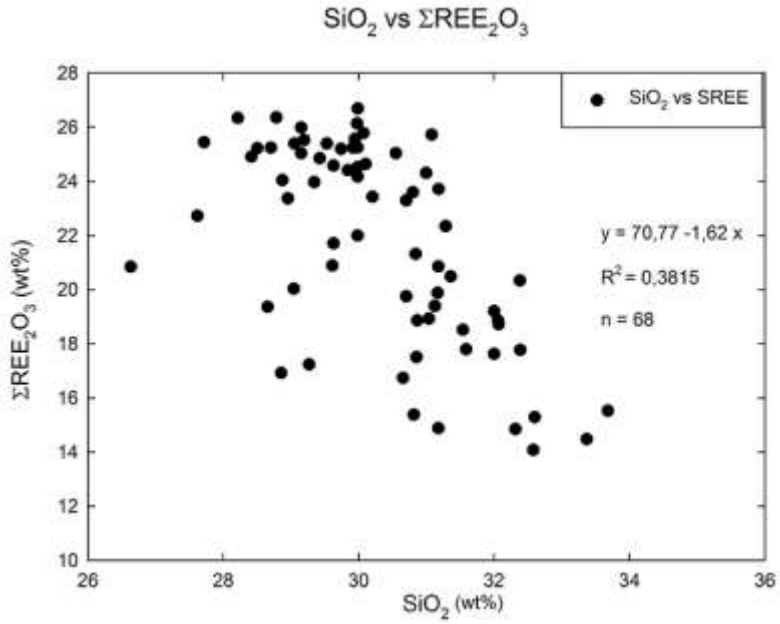

Preprints (www.preprints.org) | NOT PEER-REVIEWED | Posted: 18 September 2020

Appendix C1. Histograms of CaO in allanites.

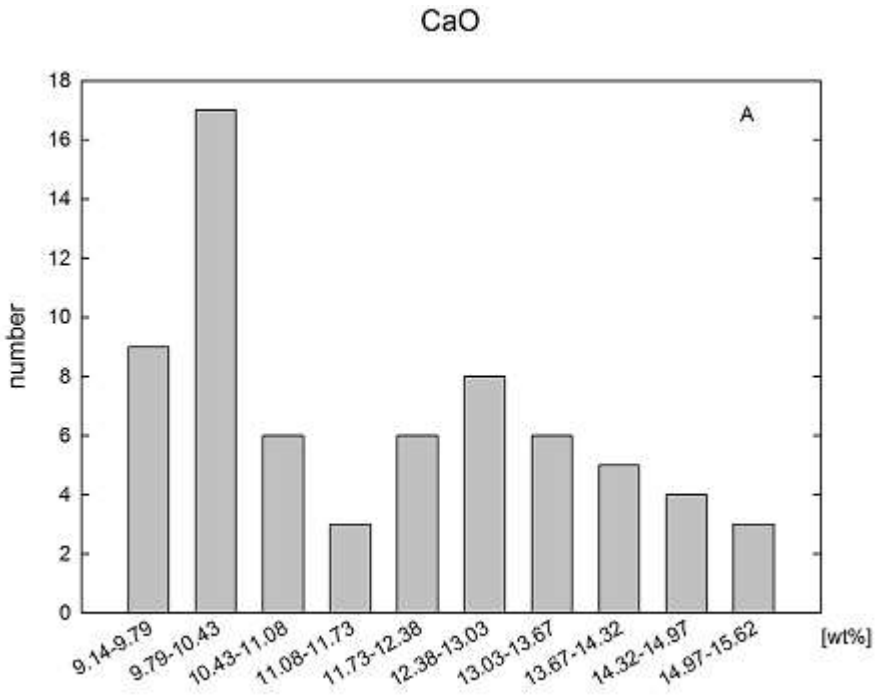

Appendix C2. Histograms of Al_2O_3 in allanites

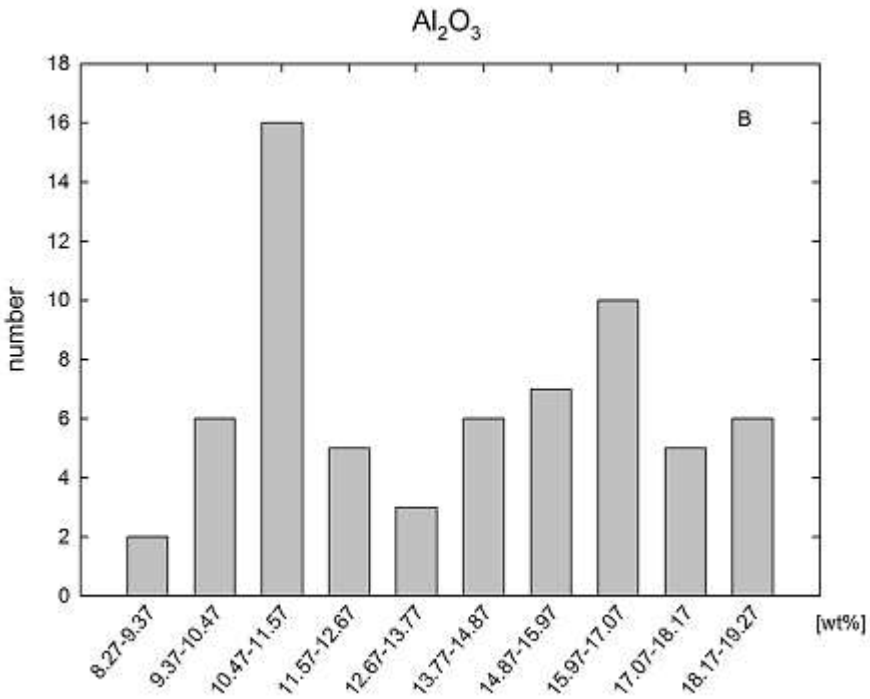

Preprints (www.preprints.org) | NOT PEER-REVIEWED | Posted: 18 September 2020

Appendix C3. Histograms of FeO in allanites

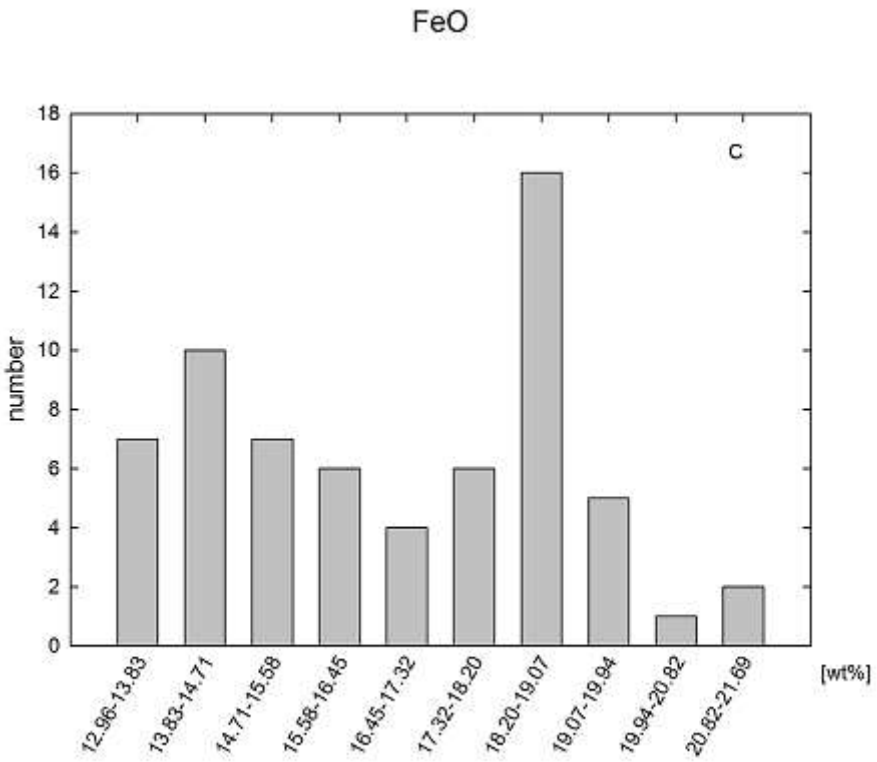

Appendix C4. Histograms of ΣREE

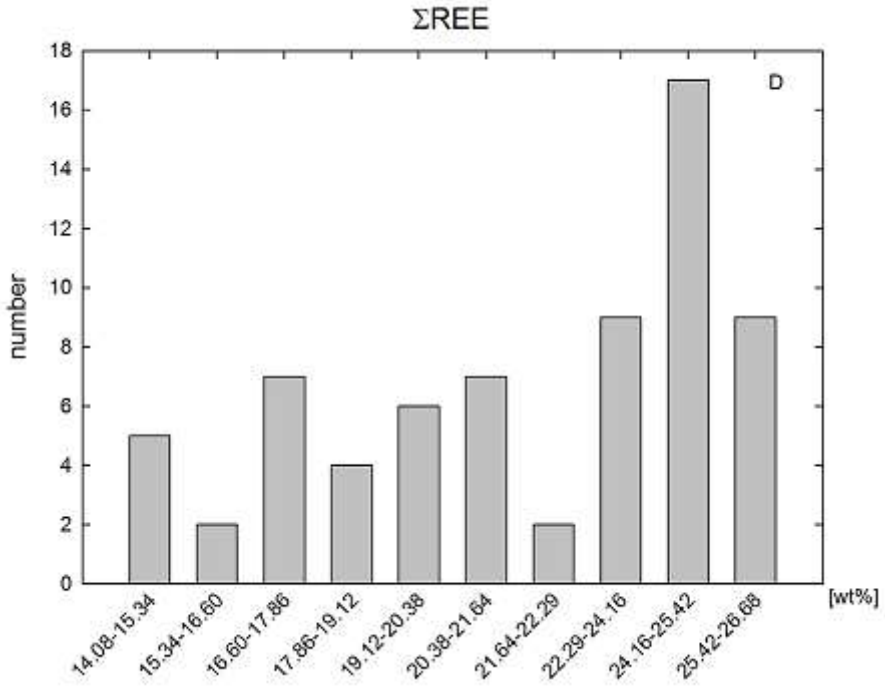

Preprints (www.preprints.org) | NOT PEER-REVIEWED | Posted: 18 September 2020

Appendix C5. Histograms of SiO_2 in allanites

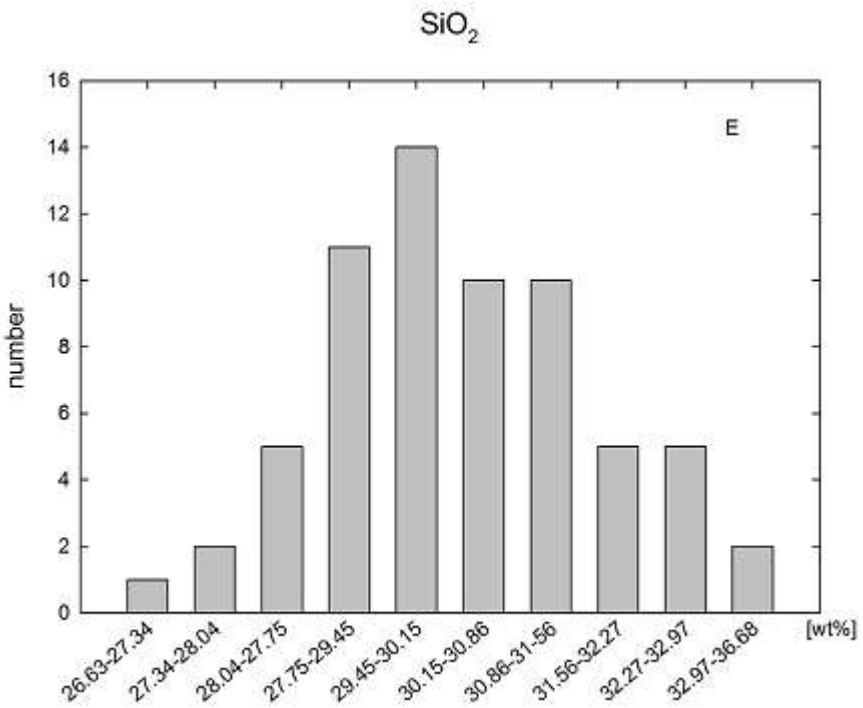

References

1. Pham, N.C.; Ishiyama, D.; Tran, T.A.; Sera, K. Mineralogical and geochemical characteristics of rare metals bearing Na Bop, Lung Hoai, Nason and Sin Quyen Base metal deposits, Northern Vietnam. *NMCC Annual Report*, **2011**, 18, 49-55.
2. Gas'kov, I.V.; Tran, T.A.; Tran, T.H.; Pham, T.D.; Nevolko, P.A.; Pham, N.C. The Sin Quyen Cu-Fe-Au-REE deposit (*northern Vietnam*) composition and formation conditions. *Russian Geology and Geophysics*, **2012**, 442-456.
3. Zhao, X.F.; Zhou, M.F. Fe–Cu deposits in the Kangdian region, SW China: a Proterozoic IOCG (iron-oxide–copper–gold) metallogenic province. *Mineralium Deposita*, **2011**, 46 (7), 731-747.
4. ESCAP. Report of Economic and Social Commission for Asia and the Pacific. **1990.**
5. Ta, V.D. Report of geological surveys and their results performed at the IOCG Sin Quyen deposit in Lao Cai, North Vietnam. Main Department of Geology of Vietnam. **1975**, 318 (in Vietnamese).
6. McLean, R.N. The Sin Quyen iron oxide-copper-gold-rare earth oxide mineralization of North Vietnam. *InHydrothermal iron oxide copper-gold & related deposits: A global perspective,* Porter T.M, Ed., PGC Publishing, Adelaide, 2001, 293-301.
7. Ishihara, S.; Hideo, H.; Mihoko, H.; Pham, N.C.; Pham, T.D.; Tran, T.A. Mineralogical and chemical characteristics of the allanite-rich copper and iron ores from the Sin Quyen mine, northern Vietnam. *Bulletin of the Geological Survey of Japan*, **2011**, 62, 5/6, 197 – 209.
8. Pham, T.H. The Ngoi Chi Formation in the Phan Si Pan area of northwest Vietnam revealed by zircon U-Pb age and Hf isotope composition. *Acta Geoscientica Sinica*, **2015**, 36m, 755-760.
9. Nguyen, D.C.; Le, K.P.; Jodłowski, P.; Pieczonka, J.; Piestrzyński, A.; Duong, V.H.; Nowak, J. Natural Radioactivity at the Sin Quyen iron oxide copper gold deposit in North Vietnam. *Acta Geophysica*, **2016**, 64 (6), 2305-2321.
10. Nguyen, D.C.; Pieczonka, J.; Piestrzyński, A.; Duong, V.H.; Le, K.P.; Jodłowski, P. General characteristics of rare earth and radioactive elements in Dong Pao deposit, Lai Chau, Vietnam. *Vietnam Journal of Earth Sciences*, **2017**, 39 (1), 13-25.
11. Tran, T.H. In plate magmatism in Northern Vietnam and its metallogeny. ScD Thesis. IGM SO RAN, Novosibirsk, **2007**.
12. Li, X.C.; Zhou, M.F. Hydrothermal alteration of monazite-(Ce) and chevkinite-(Ce) from the Sin Quyen Fe-Cu-LREE-Au deposit, north-western Vietnam. *American Mineralogists*, **2017**, 102, 1525-1541.
13. Li, X.C.; Zhou, M.E.; Chen, W.T.; Zhao, X.F.; Tran, M.D. Uranium-lead dating of hydrothermal zircon and monazite from the Sin Quyen Fe-Cu REE-Au-(U) deposit, northwestern Vietnam. *Mineralium Deposita*, **2018**, 53 (3), 399-416.

Preprints (www.preprints.org) | NOT PEER-REVIEWED | Posted: 18 September 2020

14. Pieczonka, J.; Piestrzyński, A.; Le, K.P.; Nguyen, D.C.; Jodłowski, P.; Doung, V.H. Rare Earth, radioactive and selected elements in the iron oxide copper gold Sin Quyen deposit in North Vietnam. In: *Second International Conference on Scientific Research Cooperation between Vietnam and Poland in Earth Sciences*, Bach Khoa Publishing House, Hanoi, **2015**, 331-353.
15. Pieczonka, J.; Piestrzyński, A.; Nguyen, D.C.; Le, K.P.; Duong, H.V. IOCG Sin-Quyen deposit, Lao Cai, N-Vietnam. *Mineral resources to discover. 14th Biennial SGA Meeting, Quebec, Canada*, **2017**, 955-959.
16. Pieczonka J.; Chau N.D.; Piestrzyński A.; Phon L.K. Timing of ore mineralization using ore mineralogy and U-Pb dating, Iron Oxide Copper Gold Sin Quyen de posit, North Vietnam. *Geological Quarterly*, **2019**, 63(4), 861–874.
17. Li, X.C.; Zhou, M.F. The nature and origin of hydrothermal REE mineralization in the Sin Quyen deposit, Northwestern Vietnam. *Economic Geology*, **2018**, 113 (3), 645-673.
18. Tong-Dzuy, T.; Javier, P.; Ta Hoa, P. Fist suggest continental connections between the Indochina and South China blocks in Middle Devonian time. *Geology*,**1996**, 24, 571-574.
19. Lepvrier, C.; Muluski, H.; Van Vuong Nguyen; Roques, D.; Axente, V.,;& Rangin, *C*. Indosinian NW-trending shear zones within the Truong Son belt (Vietnam). ^{40}Ar-^{39}Ar Triasic age and Cretaceous to Cenozoic overprints. *Tectonophysics*, **1997**, 283, 105-127.
20. *Carter*, A.**;** *Clift***,** P. D.Was the Indosinian orogeny a Triassic mountain building or a thermotectonic reactivation event?, Comptes Rendus. *Geosciences*, ***2008*****,** 340, 83-93.
21. Faure, M.; Lepvrier, C.; Vuong, N.V.; Tich, V.V.; Lin, W.; Chen, Z. The South China block-Indochina collision: Where, when, and how? *Journal of Asian Sciences*, **2014**,79, 260-274.
22. Tran, V.T. Geology of Vietnam [the North Part]. Science and Technology Publishing House, Hanoi, **1979**,78-95.
23. Tapponnier, P.; Lacassin, R.; Leloup, H.; Scharer, U.; Zhong, D.; Liu, X.; Ji, S.; Zhang, L.; Zhong, J. The Ailaoshan-Red river metamorphic belt: tertiary left-lateral shear between Indochina and South China. *Nature*, **1990**, 343, 431-437.
24. LeLoup, P.H.; Tapponnier, P.; Lacassin, R. Discussion on the role of the Red River shear zone, Yunan and Vietnam in the continental extrusion of SE Asia. *Journal of Geological Society, London*, **2007**, 164, 1253-1260.
25. Pyle, J.M.; Spear, F.S.; Wark, D.A. Electron microprobe analysis of REE in apatite, monazite and xenotime: protocols and pitfalls. In *Reviews in Mineralogy and Geochemistry*, **2002**, 48, 337-362.
26. Seal, R. Sulphur isotope geochemistry of sulphide minerals. USGS Staff – Published Research. **2006**, 345.https://digitalcommons.unl.edu/usgsstaffpub/345
27. Ohmoto H.; Rye R.O. Isotopes of sulfur and carbon. In *Geochemistry of hydrothermal ore deposits*, 2nd, Barnes, H.L., Ed. J Wiley and Sons, New York, 1979, 509-567,
28. Dupuis, C.; Beaudoin, G. Discriminant diagrams for iron oxide trace element fingerprinting of mineral deposit types. *Mineralium Deposita*, **2011**, 46, 319-335.
29. Fengli, Y.; Yafei, W.; Shunfu, L.; Xiaofen, L.; Pengfei, G.; Jiannian, Z. Comparisons between the Zhuchong Fe-Cu Deposit in Anqing and the IOCG-type Deposits. *Acta Geologica Sinica*, **2014**, 88 (S2), 403-404.
30. Chen, W.T.; Zhou, M.F.; Gao, J.F.; Hu, R. Geochemistry of magnetite from Proterozoic Fe-Cu deposits in the Kangdian metallogenic province, SW China. *Mineralium Deposita*, **2015**, 50, 795-809.
31. Shieh, R.S.; and Duffy, T.S. Raman spectroscopy of $Co(OH)_2$ at high pressures: Implications for amorphization and hydrogen repulsion. *Physical Review, B*, **2002**, 66 134301, 1-8.
32. http://rruff.info/Allanite-(Ce)/R080044- access date: 2019-12-12
33. López, A; Frost, R.L. Identification of allanite (Ce, Ca, Y)2(Al, Fe3+)3(SiO4)3OH found in marble from Chillagoe, Queensland using Raman spectroscopy. *Spectrochimica Acta Part A: Molecular and Biomolecular Spectroscopy*, **2015**, 138, 229–233.
34. Ngo, X.D., Zhao, X.F., Tran, T.H., Deng, X-D., li, J-W. Two episodes of REE mineralization of the Sin Quyen IOCG deposit, NW Vietnam. Ore Geology Reviews, 2020, http://doi.org/10.1016/j.oregeorev.2020.103676.
35. Belperio, A.; Flint, R.; Freeman, H. Predominent Hill: A hematite dominated, iron oxide copper-gold system. *Economic Geology*, **2007**, 102, 1499-1510.
36. Williams, M.R.; Holwell, D.A.; Lilly, R.M.; Case, G.N.D.; McDonald, I. Mineralogical and characteristics of the fluorite-rich and Monakoff E1 Cu-Au deposits, Cloncurry region, Quislend, Australia: implication for regional F-Ba-rich IOCG mineralization. *Ore Geology Reviews*,**2015**, 64, 103-127.
37. Petrík, I.; Broska, I.; Lipka, J.; Siman, P. Granitoid Allanite-(Ce) substitution relations, redox conditions and REE distributions (on an Example of I-Type Granitoids, Western Carpathians, Slovakia). *Geolgia Carpathica*, **1995**, 46, 79–94.
38. Budzyń, B.; Harlov, D.E.; Kozub-Budzyń, G.A.; Majka, J. Experimental constraints on the relative stabilities of the two systems monazite-(Ce) – allanite-(Ce) – fluor apatite and xenotime-(Y) – (Y,HREE)-rich epidote – (Y,HREE)-rich fluor apatite, in high Ca and Na-Ca environments under P-T conditions of 200–1000 MPa and 450–750 °C. *Mineralogy and Petrology*,**2017**, 111, 183–217.